University of Alberta

A Developer-free Approach to Conventional Electron Beam Lithography

by

AI ZHI ZHENG

A thesis submitted to the Faculty of Graduate Studies and Research
in partial fulfillment of the requirements for the degree of

Master of Science

in

Microsystems and Nanodevices

Electrical and Computer Engineering

©AI ZHI ZHENG

Spring 2012
Edmonton, Alberta

Permission is hereby granted to the University of Alberta Libraries to reproduce single copies of this thesis and to lend or sell such copies for private, scholarly or scientific research purposes only. Where the thesis is converted to, or otherwise made available in digital form, the University of Alberta will advise potential users of the thesis of these terms.

The author reserves all other publication and other rights in association with the copyright in the thesis and, except as herein before provided, neither the thesis nor any substantial portion thereof may be printed or otherwise reproduced in any material form whatsoever without the author's prior written permission.

To my beloved parents, who sacrificed countless things to support me striving for a better future.

To my loving and caring wife, Veronica, who always trusts and supports me unconditionally.

Abstract

In order to achieve the best results possible by electron beam lithography (EBL), many aspects of the different stages of EBL have to be carefully optimized. In the exposure stage, dose, energy, aperture size, step size and working distance have to be carefully set. In the development stage, an appropriate developer formula corresponding to the resist has to be chosen, as well as development temperature, duration, rinsing and drying method. There are many challenges present in the co-optimization of the conditions mentioned above. Particularly in the development stage, resist swelling, line edge roughness (LER) and pattern collapse are the major obstacles to achieving the ultimate in resolution. What is noteworthy is that all three of these development problems are related to the liquid environment. Therefore, if there is a way to avoid liquid developers, all problems associated with the liquid behaviour will be eliminated. This thesis presents an approach that has the potential to fabricate dense structures without using liquid developers. The work was mainly conducted in the low exposure energy regimes from 1 keV to 5 keV. Two kinds of electron beam resist, 950k PMMA and ZEP 520A, were studied for their properties and behaviours throughout various processes such as optimized exposure, thermal development and reactive ion etching (RIE). So far, 70 nm half-pitch gratings have been successfully patterned on both 950k PMMA and ZEP 520A without liquid development. This validates a concept that may ultimately lead to widespread use of dry processing of EBL structures.

Acknowledgements

I am very pleased to dedicate this section to the people who have helped me in the course of my research and made this thesis possible.

First of all, I want to express my most sincere gratitude to my supervisor Dr. Steve Dew, who provided me with the opportunity to study in Canada. Thank you Dr. Dew, for having confidence and trust in me, and for your guidance and support. I would also like to express my gratitude to my other supervisor Dr. Maria Stepanova who spent a lot of her precious time with me engaging in many discussions and encouraging me whenever challenges arose.

I also want to extend my gratitude to my colleagues. Since the beginning of my research, Mohammad Ali Mohammad has always been kind-hearted and helpful. As a beginner in the nanofabrication field, my learning improved thanks to his hands-on demonstrations and assistance. Throughout my research, Mohammad has always been the first go-to person for advice and peace of mind especially when things went wrong. I would also like to give thanks to another senior group member, Mustafa Muhammad, from whom I also learned a lot and with whom I did my IPA:WATER work.

Most of my research work was performed at the University of Alberta's Nanofab. Thanks to the kindness and friendliness of the nanofab staff, I spent many happy working hours there. In particular, I would like to thank Jolene Chorzempa,

Stephanie Bozic, Scott Munro, Bob Brebber and Les Schowalter for their assistance in training and sharing of their expertise. Thanks to Steve Buswell for the electron beam lithography training and help as well as his suggestions on the Cryo-etch process. Thanks to Daniel Salamon at the National Institute for Nanotechnology for his assistance with scanning electron microscopy. Thanks to Shiau Yin Wu at the Integrated Nanosystems Research Facility for atomic force microscopy training and help. Many thanks also to Dr. Ken Westra for lending his PhD thesis to me and sharing his expertise on atomic force microscopy.

Finally I would like to thank all the nanofabrication group members under Dr. Dew and Dr. Stepanova's supervision and all my fellow students whom I met during my study for their assistance and friendship.

Table of Contents

1 INTRODUCTION 1

2 ELECTRON BEAM LITHOGRAPHY 4

2.1 Electron Beam Lithography (EBL) 4

2.2 Conventional EBL Process 7

2.2.1 Sample preparation 7

2.2.2 Exposure & Development 8

2.2.3 Pattern transfer 12

2.3 Electron beam resist 13

2.3.1 Positive-tone resists 14

2.3.1.1 PMMA 14

2.3.1.2 ZEP 15

2.3.2 Negative-tone resists 18

2.3.2.1 HSQ 18

2.3.2.2 Negative-tone PMMA 19

2.4 Liquid development of polymer resists 19

2.4.1 Popular developers 20

2.4.1.1 MIBK:IPA 20

2.4.1.2 IPA:H_2O 21

2.4.2 Temperature 22

2.4.3 Development Time 24

2.4.4 Drying 24

3 MOTIVATIONS FOR A DEVELOPER-FREE APPROACH 26

3.1 Challenges of liquid development environment 26

3.1.1 Pattern collapse 26

3.1.2 Swelling 28

3.1.3 Edge roughness 28

3.2 Motivations 29

3.2.1 The enlightenment 30

3.2.2 The plan 31

4 EXPOSURE OPTIMIZATION 32

4.1 Common sample preparations...32

4.2 Data acquisition by AFM...32

4.3 Dose Dependency 35

4.4 Energy Dependency 41

4.5 Initial Film Thickness Dependency 44

5 POST-EXPOSURE PROCESSING 48

5.1 Heating..49

5.1.1 Heating of PMMA samples 49

5.1.2 Heating of ZEP samples..59

5.2 Reactive Ion Etching...63

5.2.1 Normal RIE process...63

5.2.1.1 Preliminary RIE tests for both PMMA & ZEP samples 63

5.2.1.2 Effect of exposure voltage on RIE (PMMA samples) 65
5.2.1.3 Effect of RIE parameters (PMMA samples) 66
5.2.1.4 RIE for ZEP samples 68
5.2.2 Cryo-etch process 70
5.2.2.1 Cryo-etch for PMMA samples 70
5.2.2.2 Dose dependency during cryo-etch for PMMA samples 73
5.2.2.3 Cryo-etch for ZEP samples 76
6 HIGH RESOLUTION TRIALS 79
6.1 Challenges during SEM imaging 79
6.2 70 nm half-pitch gratings 80
6.3 Developer-free vs. Liquid development 81
7 CONCLUSIONS & OUTLOOK 83
7.1 Conclusions 83
7.2 Outlook 84
8 REFERENCES 87

List of Tables

Table 4.1 Experimental conditions and numerical results for dose dependency of ΔT and η 36

Table 4.2 Experimental conditions and numerical results for energy dependency of ΔT and η 41

Table 4.3 Experimental conditions and numerical results for initial film thickness dependency of ΔT and η 45

Table 5.1 Experimental conditions and numerical results for PMMA heating dependency studies 50

Table 5.2 Experimental conditions and numerical results for ZEP heating dependency studies 60

Table 5.3 Experimental conditions and numerical results of preliminary RIE tests for PMMA samples..................... 64

Table 5.4 Experimental conditions and numerical results of preliminary RIE tests for ZEP samples..................... 65

Table 5.5 Experimental conditions and numerical results of RIE for PMMA samples exposed at 5 and 20 keV 66

Table 5.6 Experimental conditions and numerical results of the effects of RIE conditions on PMMA samples 68

Table 5.7 Experimental conditions and numerical results for CF_4:O_2 RIE test on ZEP sample 69

Table 5.8 Experimental conditions and numerical results of first cryo-etch on PMMA sample 71

Table 5.9 Experimental conditions and numerical results of dose dependency during cryo-etch for PMMA sample 74

Table 5.10 Experimental conditions and numerical results of cryo-etch for ZEP samples and the effect of etching time interval 76

List of Figures and Illustrations

Figure 2.1 Patterning of electron sensitive resists [15] 5

Figure 2.2 Pattern Transfer Techniques [15] 6

Figure 2.3 The effect of dose and interline distance on positive resist morphologies. SEM images of 30 nm, 40 nm, 50 nm, and 70 nm gratings fabricated in a 65-nm thick PMMA layer on a silicon substrate, with 10 keV electrons, at various area doses. The gratings were developed for 5 sec. in a 1:3 MIBK:IPA solution at room temperature. The lateral size of all images is 1 μm × 1 μm [6, 16]. 11

Figure 2.4 Generic reaction paths of radiation damage in PMMA. Schematic diagrams showing generic reaction paths for radiation damage in PMMA. Not all possible radical intermediates, indicated by (•), are shown. (a) Abstraction of H from the main chain via b elimination with removal of the ester group. The PMMA repeat unit is also indicated. (b) Scission of the main chain by (i) removal of the ester group, leading to a terminal = CH_2, or by (ii) a direct process. The radical species can undergo further reaction or decomposition (not shown). [80-83] 16

Figure 2.5 Chemical structure of a monomer unit of ZEP 520A. Schematic of the chemical structure of ZEP 520A, a copolymer of α-chloromethacrylate and α-methylstyrene [89]. 17

Figure 2.6 Cross-linking in HSQ under the electron beam exposure [90]........... 19

Figure 3.1 Surface tension (capillary force) induced pattern collapse. The surface tension of the liquid pulls the pattern walls towards each other and hence the collapse occurs. 27

Figure 3.2 Examples for collapsed dense gratings in PMMA, imaged by cross-sectional profiles (left) and plan-view (right) [6]. 27

Figure 3.3 An example of line edge roughness. [121] 29

Figure 4.1 Example of AFM data acquisition. AFM images of 63 nm 950k PMMA on Si, exposed at 3 keV at 600 μC/cm^2, without development. (a) Flattened top view; (b) Bearing Analysis; (c) Section Analysis. 34

Figure 4.2 Dose dependencies of ΔT. Sample was 950k PMMA on Si, no development. 1 keV Base dose = 33 μC/cm^2 ; 3 keV Base dose = 100 μC/cm^2. Fittings are logarithmic except for initial T = 63 nm 1 keV, which is linear. *Dose factor equals dose normalized to the base dose at each energy level. **Multiple-pass: higher dose is achieved by exposing the same area multiple times the base dose... 37

Figure 4.3 Dose dependencies of η. Sample was 950k PMMA on Si, no development. 1 keV Base dose = 33 μC/cm^2 ; 3 keV Base dose = 100 μC/cm^2. Fittings are exponential. *Dose factor equals dose normalized to the base dose at each energy level. **Multiple-pass: higher dose is achieved by exposing the same area multiple times the base dose. 38

Figure 4.4 Energy dependency of ΔT. Sample was 62±1 nm 950k PMMA on Si, exposed at doses proportional to energy, no development. Base dose = 73.3 $\mu C/cm^2$ at 1 keV. In the fit formula, $\alpha = 0.66$ and A = 4.17 eV. The error of AFM experimental data points is ±2 nm. 42

Figure 4.5 Energy dependency of η. Sample was 62±1 nm 950k PMMA on Si, exposed at doses proportional to energy, no development. Base dose = 73.3 $\mu C/cm^2$ at 1 keV. In the fit formula, $\alpha = 0.66$ and A = 4.17 eV. 43

Figure 4.6 Initial film thickness dependencies of ΔT. Sample was 950k PMMA on Si, exposed at 3 keV, no development. Diamonds: 400 $\mu C/cm^2$; Squares: 600 $\mu C/cm^2$. 45

Figure 4.7 Initial film thickness dependencies of η. Sample was 950k PMMA on Si, exposed at 3 keV, no development. Diamonds: 400 $\mu C/cm^2$; Squares: 600 $\mu C/cm^2$.. 46

Figure 5.1 Heating influence on ΔT for PMMA. Sample was 950k PMMA on Si, no development. 3 keV Base dose = 100 μC/cm2. *Dose factor equals dose normalized to the base dose at each energy level..................... 51

Figure 5.2 Heating influence on η in PMMA. Sample was 950k PMMA on Si, no development. 3 keV Base dose = 100 $\mu C/cm^2$. *Dose factor equals dose normalized to the base dose at each energy level. 52

Figure 5.3 Comparison for no heating vs. heating. All samples were 950k PMMA on Si, exposed at 3 keV. Top view and cross-section view,

respectively. (a-b) T_0 = 31 nm, 1000 μC/cm^2, no heating. ΔT = 11 nm. (c-d) T_0 = 35 nm, 600 μC/cm^2, 105 °C for 1 min. ΔT = 21 nm. (e-f) T_0 = 31 nm, 1000 μC/cm^2, 282 °C for 30 min. ΔT = 15 nm. Squares in the center are 5-6 nm in height. 54

Figure 5.4 Thickness reduction and shape distortion under heating. 950k PMMA samples with initial film thickness T_0 = 35 nm, exposed at 3 keV, (a) 100 μC/cm^2 ; (b) 200 μC/cm^2 ; (c) 400 μC/cm^2 ; (d) 600 μC/cm^2 ; and heated at 290 °C for 15 s. 55

Figure 5.5 Effect of heating time. PMMA sample with T_0 = 35 nm, exposed at 3 keV, both at 400 μC/cm^2, heated at 285 °C for (a) 1min ; (b) 5 min. 56

Figure 5.6 Optimum exposure dose when heating for ΔT. Sample was 950k PMMA on Si, no development. 3 keV Base dose = 100 μC/cm^2, heating time was 1 min for both samples. The temperature for unheated sample was presumed to be 23 °C.. 58

Figure 5.7 Optimum exposure dose in heating for η. Sample was 950k PMMA on Si, no development. 3 keV Base dose = 100 μC/cm^2 heating time was 1 min for both samples. The temperature for unheated sample was presumed to be 23 °C.. 59

Figure 5.8 Heating influence on ΔT in ZEP. Sample was ZEP 520A on Si, no development. 3 keV Base dose = 25 μC/cm^2. *Dose factor equals dose normalized to the base dose at each energy level. 61

Figure 5.9 Heating influence on η in ZEP. Sample was ZEP 520A on Si, no development. 3 keV Base dose = 25 μC/cm^2. *Dose factor equals dose normalized to the base dose at each energy level. 62

Figure 5.10 Dose dependency for CF_4:O_2 RIE test on ZEP sample. 69

Figure 5.11 Morphology of resist after cryo-etch. 950k PMMA on Si, exposed at 3 keV, 1000 μC/cm_2, no development. 1 μm squares and 500 nm lines with 500 nm spacing, respectively. (a-b) Before ICPRIE, initial film thickness = 106 nm, ΔT = 38 nm. (c-d) After ICPRIE at -110 °C, de-scum at 5 mTorr, O_2 = 20 sccm, ICP = 150 W, RF = 20 W, 5 s, etching at 7.5 mTorr, SF_6:O_2 = 45:10 sccm, ICP = 400 W, RF = 6 W, 60 s, film thickness = 34 nm, ΔT = 20 nm. 72

Figure 5.12 ICPRIE dose dependency for ΔT. Sample was 131 nm 950k PMMA on Si, exposed at 3 keV with no development. ICPRIE was performed at -110 °C, de-scum at 5 mTorr, O_2 = 20 sccm, ICP = 150 W, RF = 20 W, etching at 7.5 mTorr, SF_6:O_2 = 45:10 sccm, ICP = 400 W, RF = 6 W. The process comprised 10 s de-scum and 60 s etch followed by another 10 s de-scum and 30 s etch. 75

Figure 6.1 70 nm half-pitch gratings on PMMA and ZEP. SEM images of 70 nm half-pitch gratings exposed at 3 keV, 7.5 μm aperture, no development, on (a) 72 nm 950k PMMA on Si, ~ 600 μC/cm2 (b) 64 nm ZEP 520A on Si, ~ 100 μC/cm^2. The dose range of the PMMA sample

was from 100 to 900 μC/cm^2 and the ZEP sample was from 25 to 225 μC/cm^2. 80

Figure 6.2 Developer-free vs. Liquid development 81

List of Symbols, Abbreviations and Nomenclature

Symbol	Definition
AFM	atomic force microscopy
Al	aluminum
Cl	chlorine
CO_2	carbon dioxide
E-beam	electron beam
EBL	electron beam lithography
eV	electron volts
GaAs	gallium arsenide
HSQ	hydrogen silsesquioxane
IC	integrated circuit
ICP	inductively coupled plasma
IPA	isopropyl alcohol
LER	line edge roughness
MEMS	microelectromechanical systems
MIBK	methyl isobutyl ketone
PMMA	poly-methyl-methacrylate
RIE	reactive ion etching
SEM	scanning electron microscopy
Si	silicon
SiO_2	silicon dioxide

T_0	initial film thickness
T_g	glass transition temperature
ΔT	raw height difference between exposed and unexposed areas
η	a parameter used to describe how effective the electron beam is in reducing the film thickness per unit dose

1 INTRODUCTION

Lithography (from Greek λίθος - lithos, 'stone' + γράφειν - graphein, 'to write') is a method for printing using a stone (lithographic limestone) or a metal plate with a completely smooth surface. Its process as described in Encyclopedia – Britannica is:

> *"In the lithographic process, ink is applied to a grease-treated image on the flat printing surface; nonimage (blank) areas, which hold moisture, repel the lithographic ink. This inked surface is then printed – either directly on paper, by means of a special press (as in most fine-art printmaking), or onto a rubber cylinder (as in commercial printing)."* [1]

In the semiconductor industry, the stone is a silicon wafer and the pattern is written on polymer which is known as resist [2]. Lithography is a very important and widely used method that is employed in the fabrication of, for example, integrated circuits (IC), microelectromechanical systems (MEMS) and microfluidics.

There are many kinds of lithography. To name a few, they include photolithography, X-ray lithography, extreme ultraviolet lithography, charged-particle lithography, neutral particle lithography, nanoimprint lithography,

scanning probe lithography, dip-pen nanolithography, magneto-lithography and so on. Among all of its variants, electron beam lithography is probably the most popular for the formation of arbitrary nanoscale structures.

In conventional positive tone electron beam lithography (EBL) processing, liquid developers are used to remove exposed broken-up resist through the dissolution of smaller and more soluble fragments of the resist. However, liquid development introduces challenges such as optimization of developer formulation, time, temperature, etc. In addition, dense structure definition is limited by factors such as resist swelling and capillary force induced pattern collapse. Hence, a simplified development process that avoids liquid development could be quite attractive for EBL patterning of dense structures.

At the beginning of this thesis in Chapter 2, I briefly introduced the EBL technique in general. Then I have outlined the knowledge and research that are most relevant to my thesis work as well as the challenges in the field and reported attempts of solving them. In Chapter 3, I elaborated on the motivation and the possibilities of developing an approach that would completely avoid the liquid development and then laid out a plan for my experiments. In Chapter 4, I investigated the influence of exposure dose, energy and initial film thickness on the thickness reduction during exposure. After that, in Chapter 5, I further explored the effect of post-exposure heating and reactive ion etching as strategies to assess the viability of a development procedure that completely avoids the use

of liquids. Then, in Chapter 6, I described my attempts to create high resolution dense gratings by using the developer-free approach. I also compared the results with that of conventional liquid development. Finally, in Chapter 7, I summarized the observations of my experiments and suggested possible improvements that can be further explored in the future.

2 ELECTRON BEAM LITHOGRAPHY

2.1 Electron Beam Lithography (EBL)

EBL is the most mature lithographic technique of all the alternatives to conventional photolithography [3], thanks to its long research and application history. Since 1967 [4, 5], EBL has been widely studied in many industrial, educational and governmental institutions. EBL is the major [6] nanoscale resolution capable, maskless [7] direct write lithographic technique. It utilizes a narrow focused electron beam to create patterns on a layer of electron sensitive resist through electron irradiation [6]. The energy level of electrons ranges from a few hundred electron volts (eV) [8-10] to about 100 keV [11-14].

Conventional EBL processes are comprised of four main stages: sample preparation, electron beam exposure, development and pattern transfer. The most critical stages for performance are the exposure stage and the development stage.

A simple illustration of the process is shown in Figure 2.1 and Figure 2.2. As shown in Figure 2.1, a layer of electron sensitive resist, in this case PMMA, is first spin-coated onto a substrate (e.g. silicon, silicon dioxide, all type of semiconductors and metals, glass) and baked to harden the film and drive off the solvent; second, selected areas of the resist is exposed under the electron beam; third, the sample is immersed in a developer to selectively remove the resist from the exposed area [15].

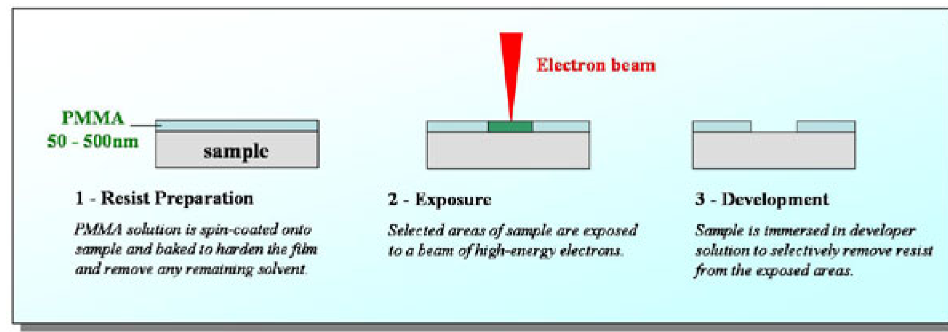

Figure 2.1 Patterning of electron sensitive resists [15]

There are many factors that affect the resolution of EBL. In the exposure stage, avoiding unwanted exposure of the resist is the key. Such unwanted exposure is mainly caused by forward scattering (broadening of the beam due to scattering of the primary electrons), generation of secondary electrons and backscattering (electrons back scattered from the substrate resulting in exposure at distances much greater than the beam diameter, also known as the proximity effect) [6, 16, 17]. In the development stage, challenges are resist swelling [18-25], pattern collapse [26, 27], micellization [6, 16] and line edge roughness (LER) [28]. Most of these problems are associated with the liquid development environment.

After development, the temporary resist pattern is transferred into the substrate, typically either by lift-off or etching as shown in Figure 2.2 [15]. In the metal lift-off process, a thin layer of metal, such as aluminum (Al), is sputtered or evaporated onto the developed resist. Then the sample is immersed into a solvent that dissolves the remaining resist and the metal is therefore “lifted off” [15] expect where it directly contacts the substrate. For PMMA, acetone is commonly

used as the solvent during lift-off. In the reactive ion etching process, certain gas species are chosen to selectively etch the exposed materials while at the same time avoid etching the patterned resist as much as possible. In this example, a plasma based on chlorine (Cl) gas is used as the etchant. After all the exposed metal is etched away, the protective resist layer can be removed.

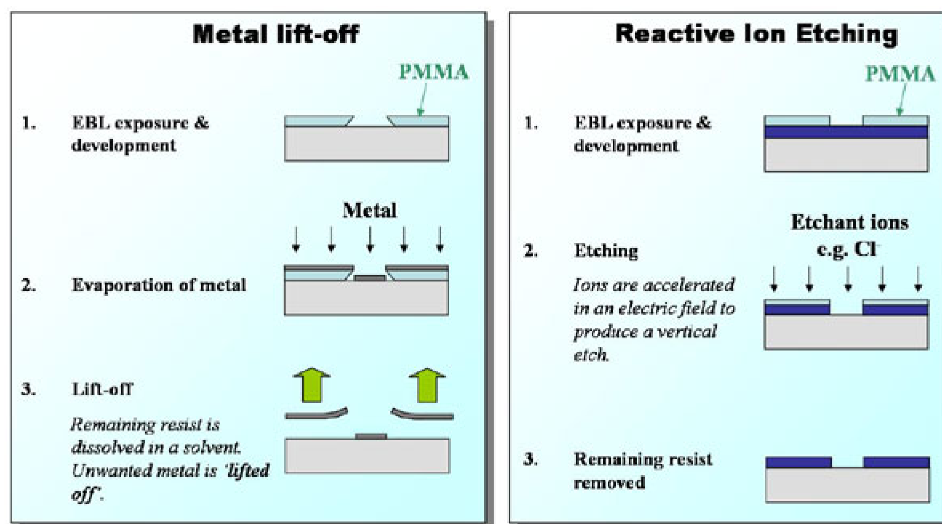

Figure 2.2 Pattern Transfer Techniques [15]

EBL has been mainly used for mask making for optical lithography and for directly writing on the wafer [29] and has a broad range of applications such as in the field of photonics, electronics, magnetic storage, microsensors, quantum communication, nanotubes and nanowires and superconducting single photon detectors [7].

2.2 Conventional EBL Process

2.2.1 Sample preparation

In the sample preparation stage, the substrate has to be first piranha cleaned to ensure good adhesion of the resist [16]. Then, if the substrate is going to be spin-coated immediately after the piranha cleaning, a de-hydration bake is commonly employed. Then, according to the needs, a layer of electron sensitive resist, or sometimes different layers of materials [30-34], is spin-coated by a spinner onto the substrate. Commonly used substrate materials are silicon (Si), silicon on insulator (SOI) such as silicon on silicon dioxide (SiO_2) or glass, but they can be all types of semiconductors such as gallium arsenide (GaAs) [14] and other SOIs such as silicon on sapphire [35] and quartz and sapphire [36], although less common. Initially, the resist is dissolved in a solvent to facilitate dispensing onto the substrate. The spin-coating is usually done with a high speed turntable and different thicknesses are achieved by spinning at different speeds. The higher the centripetal acceleration, the lower the remaining thickness of resist after dispensing. After the spin-coating, a pre-bake (soft bake) is required to harden the film, drive off the solvent and enhance the adhesion between resist and substrate. The baking temperature, time and ambient (e.g. pressure) varies according to the resist/materials used. Normally a hotplate is used for baking. However, other forms of baking such as vacuum hotplate/oven may provide certain advantages in some applications. Finally, the sample is inspected by

spectral reflectance or ellipsometry to make sure that the correct thickness is obtained. Then, the sample is ready for exposure.

2.2.2 Exposure & Development

Exposure and development are two separate but interdependent stages in the process. These two stages are the most important stages in the EBL process and ultimately determine the performance of the technology. All parameters in each of the stages have to be co-optimized to achieve the best result that is possible.

Design of the exposure stage starts with the definition of patterns that are to be written and the exposure parameters. There are many parameters involved during the exposure process such as aperture size, beam diameter, beam current, step size, aperture alignment, stigmation and working distance. The most critical parameters in this stage are exposure energy and dose.

During the exposure, a layer of electron sensitive material (resist) is exposed by a focused electron beam at designated locations. The electron exposure induces a chemical change in the material. For positive tone resist such as PMMA, chain scissioning occurs and the exposed resist becomes more soluble in a suitable developer. For negative tone resist such as HSQ or calixarene, cross-linking occurs and the exposed resist becomes more resistant to dissolution. [6]

Generally, higher exposure voltages could achieve higher resolution more easily as a result of less forward scattering of electrons as they travel through the resist [37]. However, at the same time, higher voltages also have more extensive back scattering of electrons from the underlying substrate which leads to broadening and the so-called proximity effect [6, 37]. The intensity and range of backscattered electrons increases with the incident voltage. At 50 keV, the range of the proximity effect is as large as 0.5 mm, causing a delocalization of exposure to the patterns over this area [17]. Meanwhile, at higher voltages, the sensitivity of the resist is reduced as electrons penetrate more deeply into the substrate and higher doses are required [38-41]. Consequently, higher voltages yield lower throughput due to increased exposure time. Also, high voltages may lead to more underlayer damage [40, 41]. On the other hand, operating at low energy has several advantages, which include higher sensitivity, reduced charging, less proximity and heating effects, reduction in substrate damage and improved throughput [6, 10, 42-44]. Routinely considered as the resolution limiting factor, the forward scattering of low energy electrons can be minimized by using thinner resist [17] or alternatively be utilized to facilitate the lift-off process [45]. Although conventionally EBL has usually been utilized at higher energy levels (typically between 30 and 100 keV), low-voltage electron beam lithography has been more prevalent in recent years thanks to the improvement in column architecture and the availability of high-density and stable electron sources such as the cold field emission source [41, 46-49].

For a given energy, the exposure dose has a huge impact on the morphologies of the exposed areas which can be characterized as under-exposure, optimum exposure and over-exposure[6, 16, 37, 44]. Under-exposure is due to the insufficient dose to fragment or cross-link the polymer to modify the resist dissolution behaviour during development. Over-exposure occurs when the given dose is so high that even the nominally unexposed regions receive enough dose to modify their dissolution behaviour and prevent development of the pattern. A good example to illustrate this impact is shown in Figure 2.3 [6, 16]. In these articles, Mohammad et al. pointed out that the quality of gratings is not only strongly dependent on the exposure dose but also on the interline distance [6, 16]. As can be seen in Figure 2.3 as well, over-exposure can result in additional morphologies such as pattern collapse and micellization.

Due to forward scattering and the proximity effects during exposure, when exposing certain shapes, the dose distribution is non-ideal. Some regions of the pattern may receive higher dose than expected and some regions may receive lower doses than expected. In order to correct for this effect, manufactures of various EBL tools have been including an automatic dose adjustment feature in their tool's software. However, this is a complex task and not always achievable. So, at times, researchers still have to do optimization manually through analyzing the effect and making corresponding modifications to the patterns when designing the exposure process [50]. An example of such modification is shown in Ref. [51] by Mohammad et al.

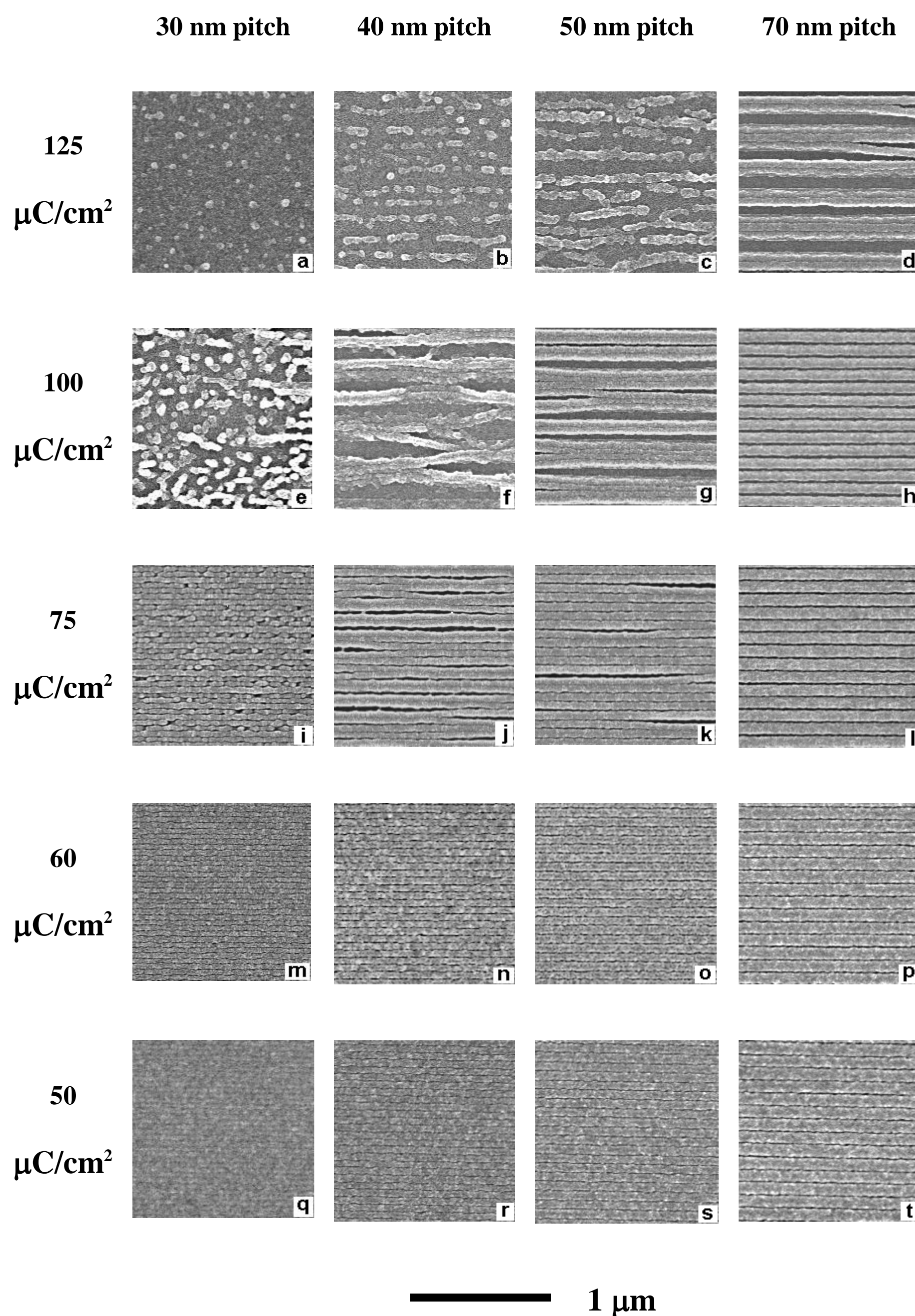

Figure 2.3 The effect of dose and interline distance on positive resist morphologies. SEM images of 30 nm, 40 nm, 50 nm, and 70 nm gratings fabricated in a 65-nm thick PMMA layer on a silicon substrate, with 10 keV electrons, at various area doses. The gratings were developed for 5 sec. in a 1:3 MIBK:IPA solution at room temperature. The lateral size of all images is 1 μm × 1 μm [6, 16].

A large amount of experimental results show that development, together with exposure, is also a crucial stage in the EBL process [6, 16, 22-24, 37, 44, 52-62]. Unlike the electron scattering in the exposure stage, the development process is difficult to predict theoretically [63], and the molecular mechanisms of development are still not fully understood [6]. The key parameters in the development stage that have been found to dramatically affect the morphologies and success of the developed structures [6] are developer formula [53, 56-58, 60, 61], duration of development [57, 64, 64], process temperature [53, 55, 58, 65] and drying method [66-70]. Detailed discussions of the above parameters can be found in the following section 2.4 Liquid development of polymer resists on page 19.

2.2.3 Pattern transfer

Pattern transfer is a process that transfers the exposed pattern from resist to the substrate or layer beneath the resist. Two commonly used pattern transfer techniques are lift-off [33, 45] and etching [71, 72].

A simple illustration and introduction to the lift-off process has been given in the section 2.2 Conventional EBL Process and Figure 2.2 on page 5. Lift-off works on the principle that the metal sticking to the substrate will not be lifted off during resist dissolution due to the adhesion to the substrate while the metal on top of the resist will be lifted off along with the resist that is stripped off from the substrate by solvent. Forward scattering of low energy EBL can also be utilized in the lift-

off process [45] as the resulting re-entrant resist profile facilitates the clean separation of metal on the substrate from that on the resist. However, since there is an essential criterion for lift-off to work successfully which is that the exposed areas have to reach clearance to the substrate, I employed lift-off in my experiments to check whether clearance is reached.

Etching is further divided into wet etch [10, 73] and dry etch such as RIE [74]. Comparing to other pattern transfer techniques, RIE is a much more complex yet promising process. In this thesis work, I have investigated the viability to combine the development and pattern transfer by RIE into a one step process. Such investigation can be found in section 5.2 Reactive Ion Etching on page 63.

2.3 Electron beam resist

Resists constitute a vast research topic, so I limited my discussions to only electron beam resist which is sensitive to electrons. The operation of EBL relies on the exposure of the resist by electrons [75]. During the exposure, the resist undergoes physicochemical modifications due to the impact of electrons. Electron beam resists are classified into positive-tone or negative-tone by their behaviours during the exposure and development, and organic or inorganic by their chemical composition. The major characteristics which define the performance of a resist include sensitivity, resolution, contrast and etch resistance [76]. Sensitivity is quantified by the minimum dose required to assure clearance

after development. Resolution is defined by the minimum feature size achievable with the resist. Contrast refers to how sharp is the transition from unexposed to exposed, which also has implications to resolution. Etch resistance is characterized by the efficiency of different etching processes. Other factors used to evaluate a resist include adhesion to different substrates and shelf life.

2.3.1 Positive-tone resists

Positive-tone resists undergo scission of bonds in the polymer chains under electron beam exposure [6, 16]. The main chain scissioning leads to a decrease in the average molecular weight [38, 77] and fragmentation of the resist is believed to be the dominating process during the exposure [6, 16, 78]. During the development, suitable solvent is chosen to preferentially dissolve the low molecular weight, small soluble fragments produced at the exposed areas [37], so that the desired pattern is obtained. A brief introduction is given here to two of the most popular positive-tone polymer resists, PMMA and ZEP.

2.3.1.1 PMMA

Poly-methyl-methacrylate (PMMA) was the first polymer tested as a resist for EBL [79]. It is still the most widely used positive-tone resist [6, 16]. This popularity is mainly because of its capability to achieve high resolution (~10 nm) and easy processing. PMMA is classified based on the average weight of the polymer chains. Most used ones are 950,000 Daltons (950K) and 495,000 Daltons (495K). Usually, higher molecular weight PMMA provides higher

resolution; however, the sensitivity is reduced [53]. The electron beam exposure induces the chain scission down to methacrylic monomers or even smaller fragments [3] although longer oligomers are still sufficiently soluble. It is generally accepted that the main process consists of a break of the main chain, although other scission mechanisms may also contribute as shown in Figure 2.4 [80-83].

2.3.1.2 ZEP

ZEP is a relatively new e-beam resist developed by Zeon Chemicals [84]. It has a few variants which are all positive-tone resist. There are corresponding thinners (solvents) available to adjust the viscosity and specific developers for each kind. Interestingly, a recent study conducted by Koshelev et al. showed that ZEP 520A can also be developed in other developers which are not made specifically for it and the performance of ZEP 520A is greatly dependent on the developers chosen [84]. The molecular weight of the ZEP 520 family is 57,000 Daltons and ZEP 7000 family is 340,000 Daltons. The most widely used ones might be ZEP 520 with o-dichlorobenzene as the solvent and ZEP 520A with anisole as the solvent and their common developer is ZED-N50 (n-amyl acetate based).

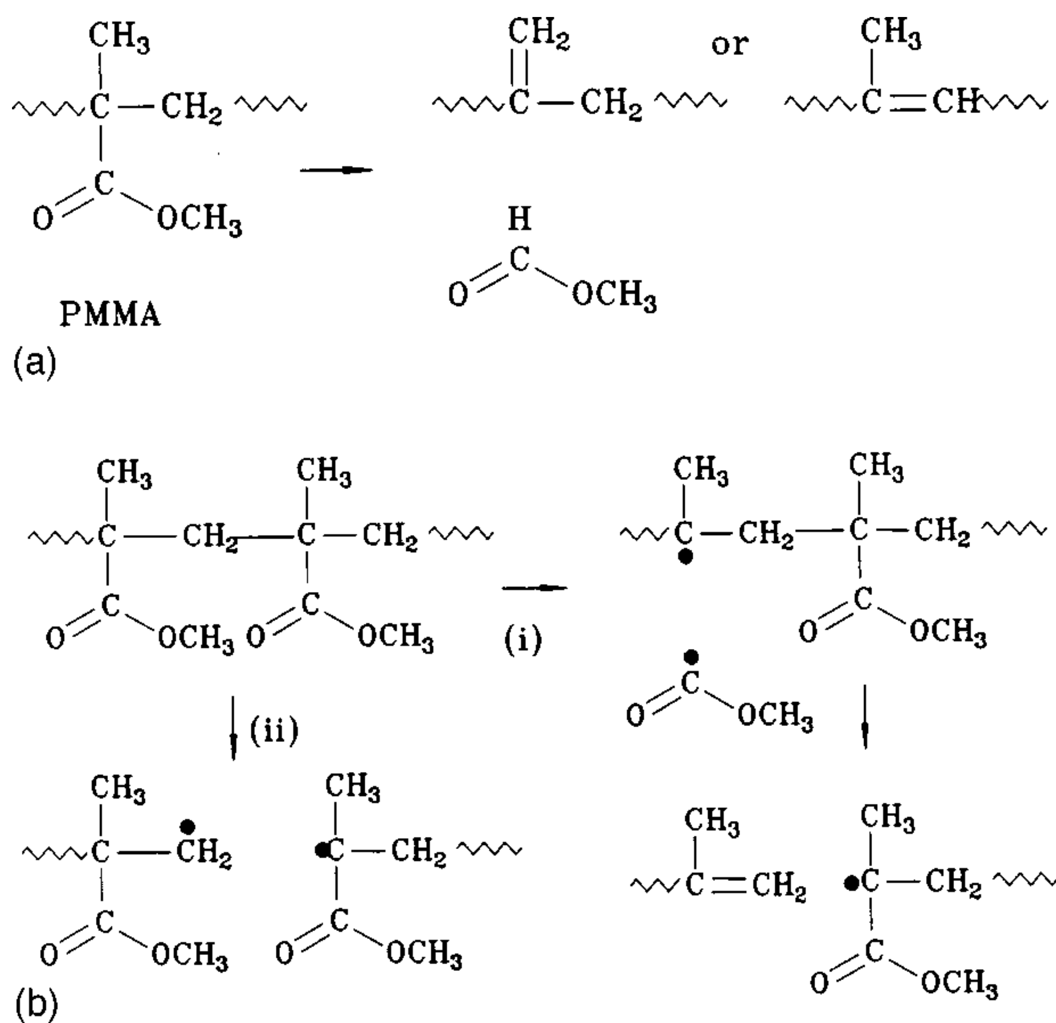

Figure 2.4 Generic reaction paths of radiation damage in PMMA. Schematic diagrams showing generic reaction paths for radiation damage in PMMA. Not all possible radical intermediates, indicated by (•), are shown. (a) Abstraction of H from the main chain via b elimination with removal of the ester group. The PMMA repeat unit is also indicated. (b) Scission of the main chain by (i) removal of the ester group, leading to a terminal = CH_2, or by (ii) a direct process. The radical species can undergo further reaction or decomposition (not shown). [80-83]

A schematic of the chemical structure of ZEP 520A is shown in Figure 2.5. Comparing to the chemical structure of PMMA, the αCl group apparently gives it a higher sensitivity and the α-methylstyrene gives it a higher dry etch resistance [85]. In comparison to the performance of PMMA, ZEP has been reported to show a higher contrast [52, 83, 84], higher sensitivity [18, 85, 86], and better dry etch resistance [85, 86]. Most techniques that are applicable to PMMA can be also applied to ZEP, for example cold development [6, 37, 44, 55, 87, 88]. It has been argued that the performance of ZEP may even exceed that of PMMA if the EBL conditions are properly optimized [84].

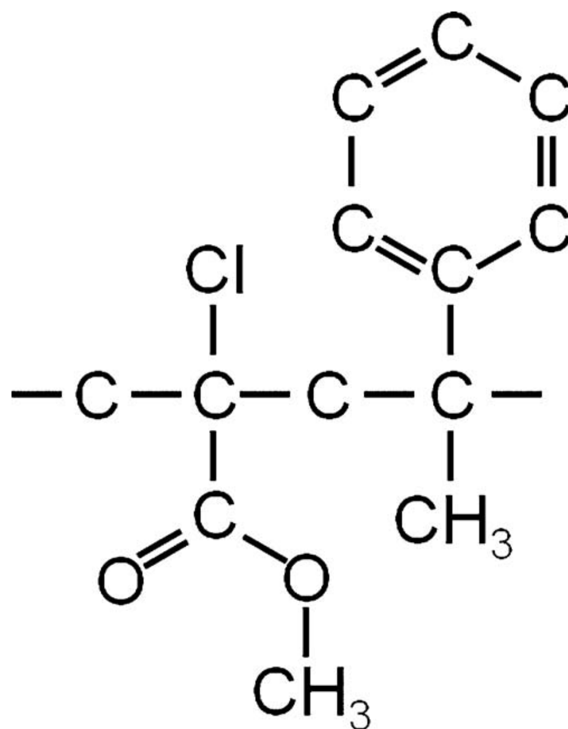

Figure 2.5 Chemical structure of a monomer unit of ZEP 520A. Schematic of the chemical structure of ZEP 520A, a copolymer of α-chloromethacrylate and α-methylstyrene [89].

2.3.2 Negative-tone resists

For negative-tone resists, such as hydrogen silsesquioxane (HSQ) or calixarene, bond cross-linking is the dominating process in the areas that are exposed by the electron beam. The cross-linking process generates structures that are locally more resistant to dissolution [6] than non-exposed areas. Consequently, after the development, exposed areas stay and non-exposed areas are dissolved.

2.3.2.1 HSQ

That HSQ can be used as a negative-tone e-beam resist was first discovered by Namatsu et al. [90-92]. HSQ is an inorganic resist that possesses many excellent features such as ultrahigh resolution [93, 94] of about 5 nm [95], minimum LER [93-98], excellent etch resistance [93-98], good stability under SEM inspection [95, 96] and small molecular size [99]. Commonly used developers for HSQ are $(CH_3)_4N(OH)$ aqueous solvent with the product of TMAH [91, 95], CD26 and so on [94, 95]. Presently, HSQ is one of the most widely used negative-tone electron beam resists [93, 94] for sub-10 nm features [91]. The limitation that prevents it from extensive applications is its relatively poor sensitivity [95].

Figure 2.6 illustrates the hypothetical mechanism of cross-linking in HSQ under the electron beam exposure. The exposure breaks the SiH bonds, which are weaker than the SiO bonds, and consequently generates cross-linking of siloxane bonds in HSQ via unstable silanols resulting from the reaction with moisture [90].

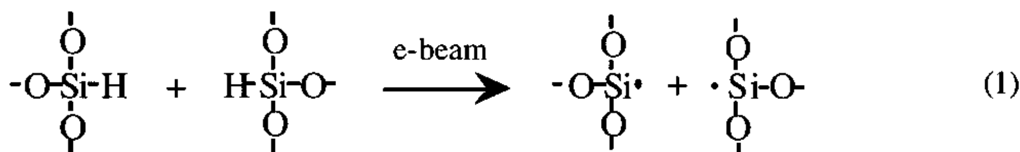

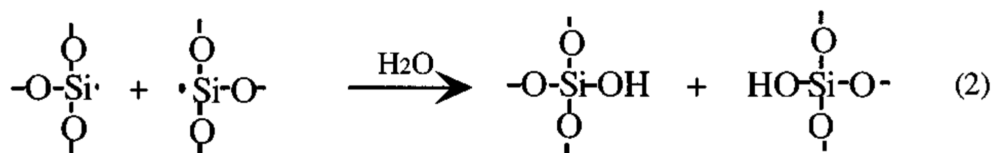

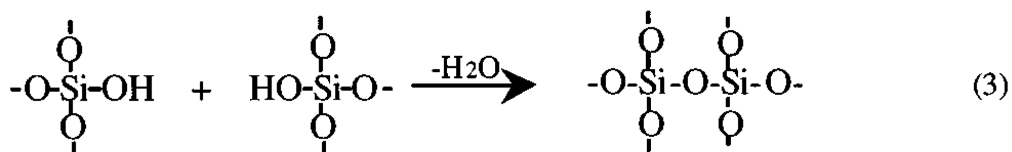

Figure 2.6 Cross-linking in HSQ under the electron beam exposure [90].

2.3.2.2 Negative-tone PMMA

Interestingly, PMMA can be also used as a high resolution negative-tone resist [100, 101]. When exposed to a high dose (>10 times of the optimum dose for positive-tone performance), PMMA undergoes cross-linking [78, 100-102] and behave as a negative-tone resist. Cross-linked PMMA is resistant to most solvents (e.g. acetone) and etchants [101]. The property of PMMA that it can perform as both positive and negative resist has been utilized for density multiplication [103-107] at the deep nanoscale.

2.4 Liquid development of polymer resists

Development is a vast and complex topic too, so I restricted my discussions to the aspects that are relevant to my thesis work. These sections focus on the liquid development of two popular polymer resists, PMMA and ZEP.

The performance of a typical development process in EBL heavily depends on the developer formula, development temperature, duration, rinsing, and drying method [19]. Molecular weight has also been found to affect the resolution achievable by development with the same kind of resist used [17]. Finally, pre-baking conditions and the solvent used to dilute/prepare the resist are factors that will also influence the overall process [19].

2.4.1 Popular developers

Developers are often a mixture of so-called solvent and non-solvent [108] or strong solvent and weak solvent. A good developer should effectively remove the exposed resist while leaving the unexposed resist intact. During the process of development, it should also cause minimum swelling and edge roughness. Below, two kinds of popular developers for PMMA are reviewed.

2.4.1.1 MIBK:IPA

When developing PMMA, methyl isobutyl ketone (MIBK) mixed with isopropyl alcohol (IPA) is a very popular choice. MIBK is a strong solvent for PMMA. IPA, on the other hand, is a very weak solvent for low molecular weight PMMA [109]. The mixing ratio between the two components has a great impact on various aspects of the development process. The sensitivity of PMMA and thickness loss of the unexposed regions decreases with decreasing MIBK concentration while the contrast increases [110]. Significant surface roughening

is observed when the concentration of MIBK exceeds 50% [20]. Particularly, MIBK:IPA = 1:3 has been found to be the optimum ratio that provides high contrast, high resolution, moderate sensitivity and almost negligible thickness loss of the unexposed regions [110]. Thus, it has been the standard developer of PMMA [111] for a long time.

2.4.1.2 IPA:H_2O

IPA:H_2O is a co-solvent (the mixture is a stronger solvent than either separate component [109]) first proposed to be a developer for PMMA in 1987 by J. M. G. Cowie et al. and high resolution has been successfully achieved for applications [60]. Separately, neither of these components can develop PMMA effectively [110], although IPA is a weak solvent and the sensitivity using pure IPA is higher than that for IPA:H2O = 7:3 [110]. The concentration of IPA and H_2O also has a similar impact on various aspects of development similarly to the case of MIBK:IPA. However, unlike MIBK:IPA, the contrast and sensitivity do not vary monotonically with the relative concentration of IPA and H_2O [110]. According to A. Olzierski and I. Raptis [110], when the relative concentration of IPA is in the 50 to 90% range, the contrast and sensitivity are high enough to be comparable with MIBK:IPA and in the range of 60 to 90%, the contrast almost stays the same. Particularly, the sensitivity of MIBK:IPA = 1:1 is the same as that of IPA:H2O = 7:3 with less thickness loss of unexposed regions in the latter case [110]. A study conducted by A. Olzierski and I. Raptis [111] also showed that three times the sensitivity is achieved for IPA:H2O = 9:1 as for MIBK:IPA = 1:3

with the development time extended to about 4 to 5 min [111]. Comparing to MIBK:IPA, IPA:H2O is believed to improve surface and line edge roughness [110], to be more reliable for the fabrication of narrow structures [17], and finally to be more environmental friendly [110].

2.4.2 Temperature

Temperature is an important parameter in the development process because both diffusion coefficient and solubility are dependent on it [19].

Conventionally, most development is processed under room temperature conditions. However, research has shown that the performance of electron beam resist such as resolution and contrast can be improved by lowering the temperature [54, 55, 65, 88, 109, 112]. L. E. Ocola et al. [65] investigated the temperature at 5 °C, M. J. Rooks et al. [109] explored the temperature range from 0 to 20 °C, and W. Hu et al. [112] examined the temperature range from 4 to 8 °C. Later, L. E. Ocola and A. Stein [55] further looked at the temperature range from −17 to +32 °C. Subsequently, B. Cord et al. [54] studied a wide temperature range from −70 to 15 °C and concluded that at approximately −15 °C is the optimum temperature for the standard MIBK:IPA = 1:3 developer. At this temperature, resolution of the resist can be greatly enhanced without significant sacrifice of sensitivity [37, 44, 54]. It is noteworthy that temperatures trend does not continue to colder. At −20 °C and below, the contrast drops dramatically.

Below about −50 °C, no development can occur [54] due to the significant drop in dissolution rate, making cold development not a useful technique anymore.

The mechanism behind cold development has been studied by many researchers. A generally accepted hypothesis is that molecular weight of the resist surrounding the exposed areas are lower than more distant unexposed regions, due to partial exposure by scattered and secondary electrons. These relatively small molecular fragments can be easily dissolved in developer at room temperature, reducing the resolution (lateral sharpness of the structure). However, at lower temperatures, these partially exposed fragments became insoluble and resolution is restored. This mechanism also explains why cold development only works for chain scission based (positive-tone) resists [54, 55, 88, 109].

Cold development is really a breakthrough in an effort to make EBL an easier, more reliable, higher resolution process. This technique is inexpensive and easy to apply [6, 37, 44, 54, 55, 88]. By varying the temperature, a trade-off between the contrast and sensitivity can be achieved [37, 44, 109]. One interesting fact is that cold development reduces the sensitivity of positive-tone PMMA but boosts the sensitivity of negative-tone PMMA [54]. Cold development has been shown to improve LER too [55]. The only disadvantage of cold development might be the higher doses required and hence longer exposure times [54].

Mohammad et al. [6, 37, 44] recently conducted research employing low-energy exposures combined with cold development in this narrow range in an effort to gain more knowledge and make potential improvements. A major finding in their work is that cold development substantially widens the applicable dose window, providing better control over properties of fabricated patterns such as aspect ratio; whereas, the decrease in sensitivity can be offset by the usage of low energy exposures [37, 44].

2.4.3 Development Time

Development time is a simple yet critical process parameter. It determines how long the resist remains in contact with developer. The rate limiting mechanism behind the effect of development time is the solvent diffusion rate which is determined by the diffusion coefficients of solvent and polymer [6, 19].

2.4.4 Drying

When drying is performed in a conventional manner, which is to blow dry with a nitrogen gun, pattern collapse is a frequently observed problem when fabricating dense structures. This collapse can be attributed to two reasons. First, the liquid trapped between dense structures has a surface tension that can cause collapse. Second, when the liquid effuses out of the structures, it carries away the aggregated polymers and produces a certain degree of sidewall roughness, which in turn destabilizes the fine resist structures and eventually can lead to collapse as

well [113]. The most effective way to solve this problem is through reducing the surface tension, for example by replacing the rinsing liquid with a supercritical fluid which has zero surface tension and high diffusivity [113-115]. The reason behind zero surface tension is that supercritical fluid does not have gas/liquid interface. It can be considered as a high-density gas and a diffusible liquid at the same time [114]. A common supercritical fluid used for this purpose is supercritical carbon dioxide (CO_2) [116]. The advantage of supercritical CO_2 is that its supercritical conditions can be reached at a moderate temperatures and pressures, T_c = 31.1 °C and P_c = 7.38 MPa, respectively [115]. Supercritical drying has been shown to prevent pattern collapse, improve the mechanical stability, increase ultimate aspect ratio (2 to 3 times), potentially enhance resolution [113, 116], and improve sidewall roughness [117].

3 MOTIVATIONS FOR A DEVELOPER-FREE APPROACH

Although the conventional development stage has been studied and optimized for many years, there are still many challenges that have not yet been overcome. A brief summary of such problems and known attempts to solve them are presented below.

3.1 Challenges of liquid development environment

3.1.1 Pattern collapse

As mentioned in section 2.4.4 Drying, a major reason for pattern collapse is believed to be the surface tension of the liquid developer during drying. A simple illustration of such mechanism is shown in Figure 3.1. The surface tension of the liquid pulls the pattern walls towards each other and hence the collapse occurs. Furthermore, once the collapse happens at one point of the two gratings, it tends to zipper the rest of the gratings. An example of such "zippering effect" is shown in Figure 3.2 [6].

Although supercritical drying can offset pattern collapse to some extent, this technique has been mainly applied to HSQ and it is not similarly efficient for all resists. In addition, it also adds extra tool cost and process steps. Moreover, the

aspect ratio achievable by supercritical drying only meets the requirements of certain applications.

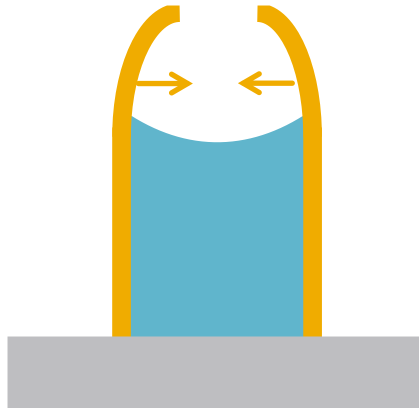

Figure 3.1 Surface tension (capillary force) induced pattern collapse. The surface tension of the liquid pulls the pattern walls towards each other and hence the collapse occurs.

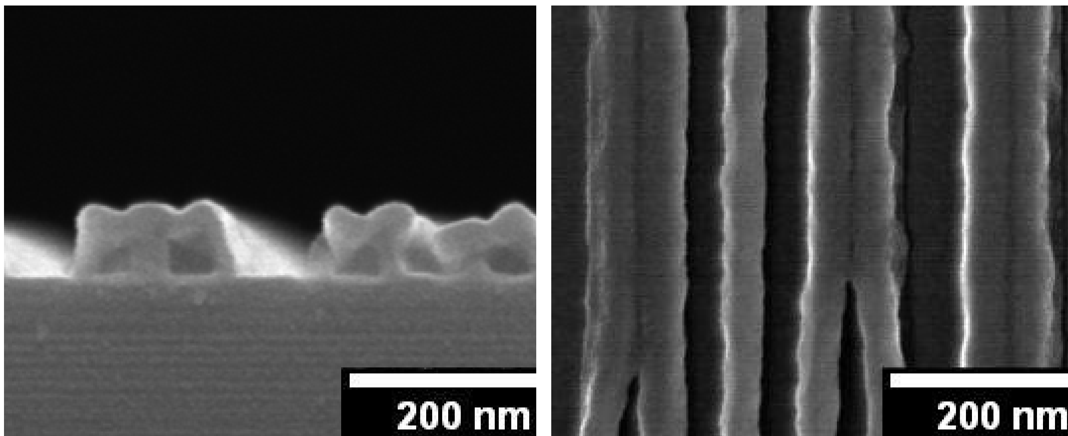

Figure 3.2 Examples for collapsed dense gratings in PMMA, imaged by cross-sectional profiles (left) and plan-view (right) [6].

3.1.2 Swelling

Swelling of partially exposed and unexposed resist during development is another challenge in EBL. Swelling is determined by solvent diffusion rate and development time [118]. The diffusion for lower molecular weight fragments is faster than that of higher molecular weight fragments [118]. Hence, the swelling is most pronounced at the partially exposed areas surrounding the exposed feature. Ultrasonic agitation is able to mitigate some swelling because the dose required to expose the resist in an ultrasonic agitation process is lower than that of conventional development process, when other development conditions are the same [118]. However, development time for ultrasonic agitation is usually longer than that of the conventional development process [17]. It is noteworthy that the mechanism of swelling [3, 108] implies that swelling cannot be completely eliminated as long as the liquid developer is involved.

3.1.3 Edge roughness

Edge roughness is another factor that limits the resolution. It has been shown that softer developer [110], cold development [55], supercritical drying [117], and ultrasonic agitation [119] are able to improve the various aspects of roughness such as surface roughness, side wall roughness, and line edge roughness. Line edge roughness is characterized by the deviation on one side of the straight line from its ideal form. It becomes a problem when the feature size is smaller than 100 nm because it affects the precision of line width and overlay control [120].

An example of line edge roughness is shown in Figure 3.3 [121]. It can be seen that the gratings in the left image have better line edge roughness than the gratings in the right image.

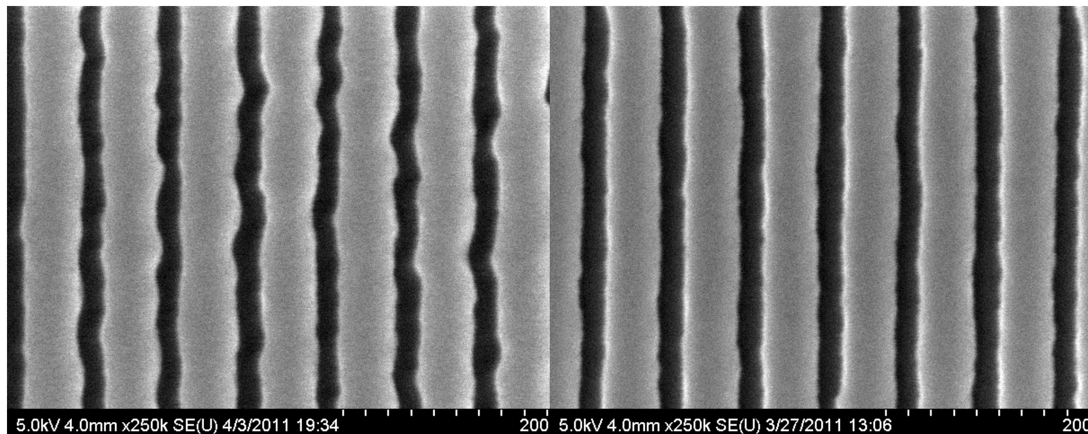

Standard Deviation along each line	Standard Deviation along each line
0.5 – 1.3 nm	**0.2 – 0.8 nm**
Best to worst case	Best to worst case

Figure 3.3 An example of line edge roughness. [121]

3.2 Motivations

As discussed in the above sections, in conventional EBL processing, liquid developers are used to remove exposed/unexposed resist through the dissolution of more soluble fragments. However, liquid development introduces challenges such as a need for optimization of developer formulation, time, temperature, etc. In addition, dense structure quality is limited by factors such as resist swelling, pattern collapse and edge roughness. Notice that these problems are largely induced by the liquid development environment. Hence, if a method can be developed such that it completely avoids the use of liquid developers, it should

also eliminate the difficulties associated with the liquid development. A simplified development process that avoids liquid development and potentially even could include pattern transfer into a one step process would be quite attractive for EBL patterning of dense structures and beneficial to the industry.

3.2.1 The enlightenment

PMMA film thickness reduction after exposure was mentioned by W. H. Teh et al. in 2003 [122]. Later, PMMA film contraction resulting in a film thickness reduction after electron beam exposure but prior to development was observed by B. Cord et al. [54] in 2007 and in his thesis 2009 [123]. More recently, H. Koop et al. [124] showed that PMMA exhibits shrinkage after the electron beam exposure. Similar observations have also been reported by M. Kotera et al. [125]. This year, the thickness reduction was observed again by S. Gorelick et al. [12]. However, more detailed research regarding to this phenomenon has not been performed.

Possible mechanisms for this effect include electron beam evaporation of resist or residual solvent, formation of volatile species through polymer fragmentation [78, 110, 126, 127], and resist densification [102, 122]. While relatively minor, this thickness reduction during electron beam exposure suggests a pathway to avoid liquid development. In this thesis work, I explored the exposure conditions in an effort to make the thickness reduction more pronounced. I also further investigated the post-exposure dry processing to extend the effect.

3.2.2 The plan

The published experiments by W. H. Teh et al. [122], B. Cord et al. [54, 123], Koop et al. [124] and Kotera et al. [125] were conducted at relatively high exposure energies between 20 to 30 keV and higher (100 keV in S. Gorelick et al.'s case [12]), and a relatively weak effect has been reported. I believe that electron-resist interactions could be enhanced at lower energies due to the higher interaction cross-section [6, 38]. This suggests that exposure energy could be an important factor in thickness reduction. Further, if electron induced fragmentation produces more volatile fragments, then post-exposure heating [128-131] should enhance this effect. Even partial thickness reduction could be sufficient, if anisotropic RIE [132-134] can preserve the height difference while the thinner resist areas are etched to clearance.

In this thesis work, a developer-free approach to create nanometer scale patterns and/or structures in the resist by electron beam exposure has been investigated. I have studied the effect of exposure dose, energy and initial film thickness on the ultimate resist thickness reduction during exposure. I have further examined the effect of post exposure heating and reactive ion etching as strategies to assess the viability of a development procedure that avoids the use of liquids. I have focused on popular PMMA and ZEP resists and compared their behaviours and characteristics through the whole process. I have employed atomic force microscopy (AFM) and scanning electron microscopy (SEM) for assessing the effectiveness of this approach.

4 EXPOSURE OPTIMIZATION

In this chapter, I have studied the effect of exposure dose, energy and initial film thickness on thickness reduction during exposure by electrons. Two popular positive tone PMMA and ZEP resists are used. Atomic force microscopy (AFM) and scanning electron microscopy (SEM) are employed for assessing the effectiveness of this approach.

4.1 Common sample preparations

The resists used were standard 950k PMMA (1 - 2 %) from MicroChem Corp and ZEP 520A (ZEP:Anisole = 1:3) from Zeon Chemicals LP. PMMA samples were pre-baked at 150 °C for 5 min on a hot plate. ZEP samples were pre-baked at 170 °C for 10 min on a hot plate. Different film thicknesses were obtained by varying spin-on conditions and measured by ellipsometry. Most exposures were at 3 keV and 10 µm aperture and with a Raith 150 EBL system unless otherwise noted. An array of 1 μm^2 squares was chosen as our standard test structure because of its ease for AFM inspection and results calculation. Grating structures down to 50 nm half-pitch were also assessed using SEM.

4.2 Data acquisition by AFM

I have used two functions, bearing analysis and section analysis [135], of a Veeco Dimension 3100 atomic force microscope, to extract height difference

information and film thickness reduction information after electron beam irradiation. Bearing analysis

> *"provides a method of plotting and analyzing the distribution of surface height over a sample. This form of analysis may be applied to the entire image, or to selected areas of the image, using a rubberband box. Moreover, regions within the selected area can be blocked out by using "stopbands" to remove unwanted data from the analysis"* [135].

In my experiments, the parameters in bearing analysis were set such that a histogram was created which gave a distribution of depth at all sampled points on the surface with zero being the highest point. Therefore, the difference between the two distribution peaks is the height difference between exposed and unexposed areas. Section analysis was used to confirm the bearing results along a single scan line. This provided a cross-sectional view of exposed pattern so that pattern distortions can be observed.

Figure 4.1 is an example of how I have studied the dependency of various experimental parameters. The sample in this experiment was 63 nm thick 950k PMMA on Si exposed at 3 keV with the dose of 600 μC/cm^2. Figure 4.1(a) is a flattened top view image with the height reference bar on the side. We can get a rough estimate of height difference from the top view and also observe the surface roughness. Figure 4.1(b) is the bearing analysis. As mentioned above, the

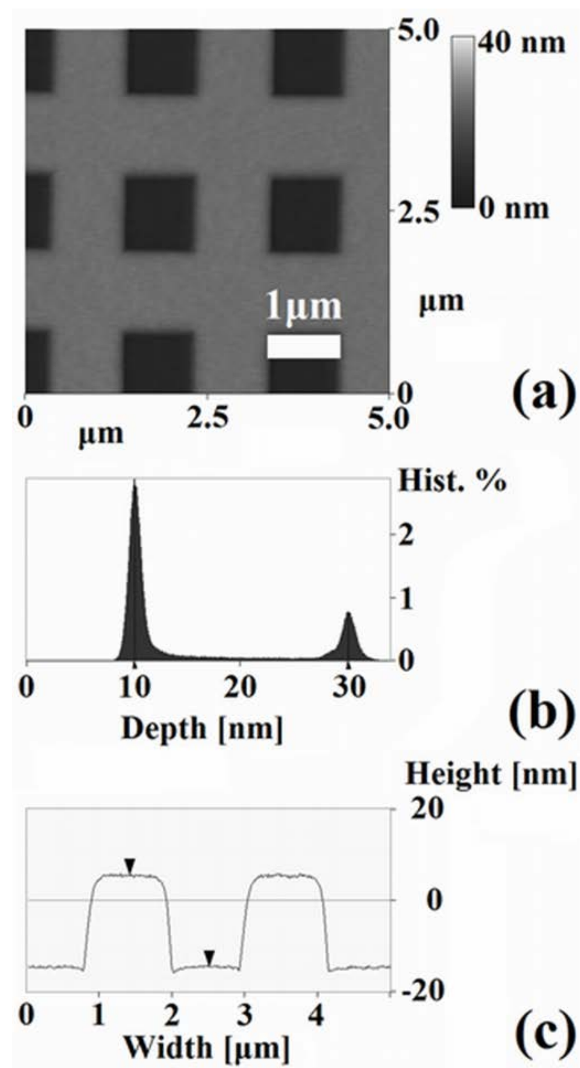

Figure 4.1 Example of AFM data acquisition. AFM images of 63 nm 950k PMMA on Si, exposed at 3 keV at 600 $\mu C/cm^2$, without development. (a) Flattened top view; (b) Bearing Analysis; (c) Section Analysis.

difference between the two peaks is the height difference between exposed and unexposed areas and this value is denoted by ΔT in the following experiments. For this particular example, ΔT is 20 nm, which is about 32% of the initial film thickness. Figure 4.1(c) is the section analysis. In addition to inspecting the

height differences of individual or average cross sections, we can also observe the change of line width, line edge roughness, surface roughness and other distortions.

4.3 Dose Dependency

To help understand the results in the following sections, I defined an etch efficiency η (mm^3/C) to describe how effective the electron beam is in reducing the film volume per unit dose. Hence, η equals to ΔT divided by area dose, where ΔT is the raw height difference between exposed and unexposed areas.

To determine dose dependency for ΔT and etch efficiency η, a series of 950K PMMA samples were exposed at the same energy but with varying doses. The base dose at 3 keV is the clearance dose required for conventional liquid development. The base doses at other energy levels were scaled proportionally to the energy to account for the energy dependence of the sensitivity [38, 44, 77]. The detailed experimental conditions and numerical results are given in Table 4.1. Plots of ΔT vs. dose factor and η vs. dose factor are given in Figure 4.2 and Figure 4.3 respectively. Initial film thickness is denoted as T_0.

Table 4.1 Experimental conditions and numerical results for dose dependency of ΔT and η

T_0 (nm)	Aperture (μm)	Energy (keV)	Dose (μC/cm^2)	Dose Factor*	ΔT (nm)	η (mm^3/C)
31	10	3	400	4	9.5	2.4
	10	3	600	6	10.6	1.8
	10	3	800	8	10.8	1.3
	10	3	1000	10	11.3	1.1
63	10	1	33	1	2.9	9.1
	10	1	66	2	5.5	8.3
	10	1	132	4	10.4	8
	10	1	198	6	14	7
	10	1	264	8	17.8	6.8
63	10	3	100	1	6	6
	10	3	200	2	10.8	5.4
	10	3	400	4	18	4.5
	10	3	600	6	20.3	3.4
63	10	3	100	1	6	6
	10	3	200**	2	10.5	5.3
	10	3	300**	3	15	5
	10	3	400**	4	18	4.5
131	20	3	200	2	20.6	10.3
	20	3	400	4	32.9	8.2
	20	3	600	6	37.4	6.2
	20	3	800	8	39.7	5
	20	3	1000	10	41.7	4.2

*Dose factor equals dose normalized to the base dose at each energy level. 1 keV Base dose = 33 μC/cm^2 ; 3 keV Base dose = 100 μC/cm^2. **Multiple-pass: higher dose is achieved by exposing the same area multiple times the base dose.

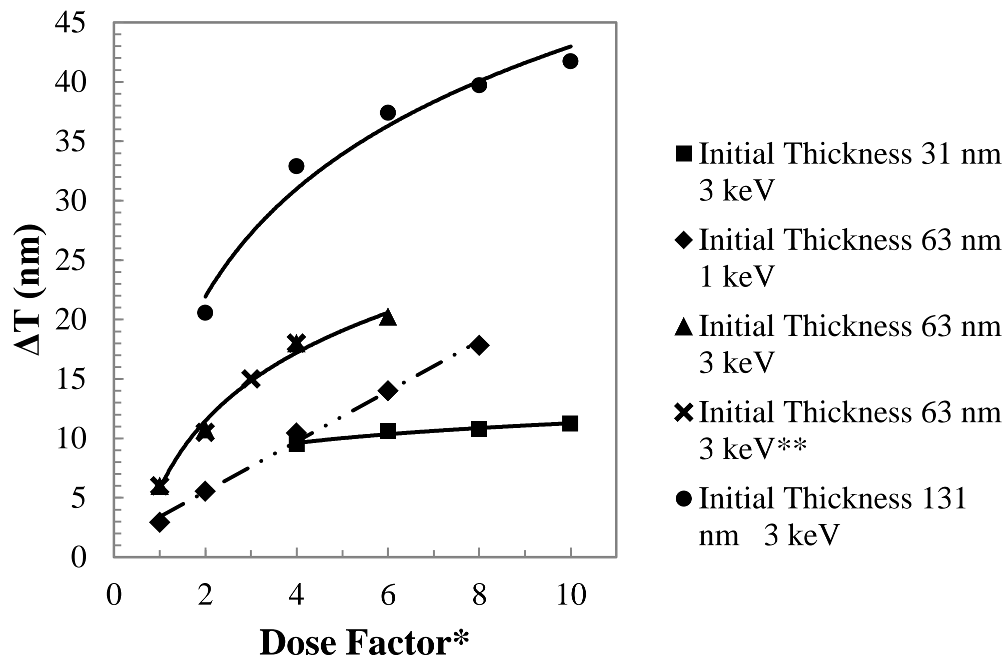

Figure 4.2 Dose dependencies of ΔT. Sample was 950k PMMA on Si, no development. 1 keV Base dose = 33 μC/cm^2 ; 3 keV Base dose = 100 μC/cm^2. Fittings are logarithmic except for initial T = 63 nm 1 keV, which is linear. *Dose factor equals dose normalized to the base dose at each energy level. **Multiple-pass: higher dose is achieved by exposing the same area multiple times the base dose.

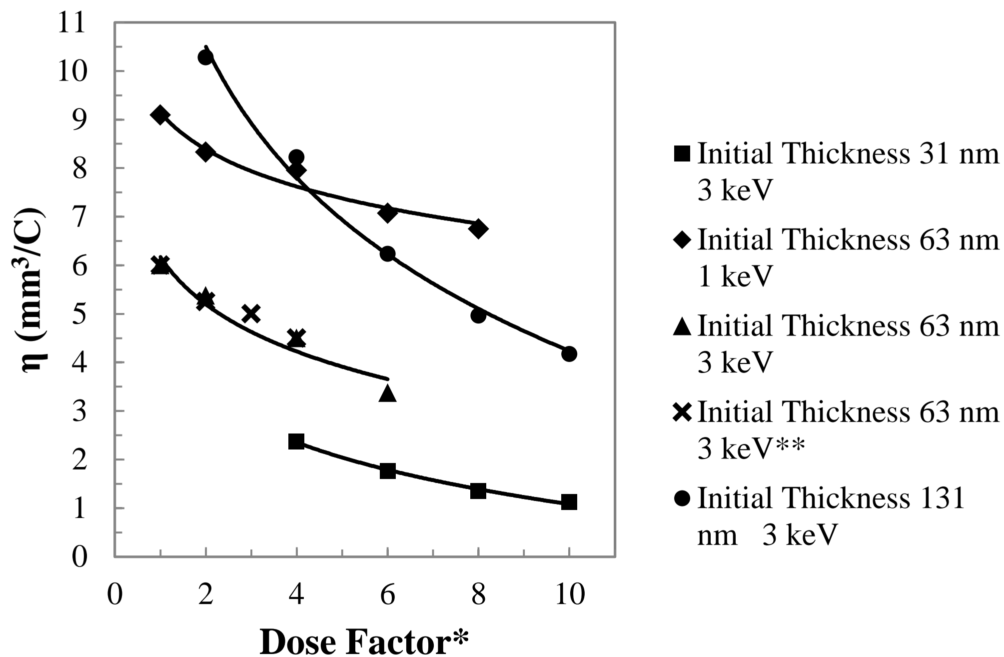

Figure 4.3 Dose dependencies of η. Sample was 950k PMMA on Si, no development. 1 keV Base dose = 33 $\mu C/cm^2$; 3 keV Base dose = 100 $\mu C/cm^2$. Fittings are exponential. *Dose factor equals dose normalized to the base dose at each energy level. **Multiple-pass: higher dose is achieved by exposing the same area multiple times the base dose.

The results in Figure 4.2 have clearly shown that dose is a very important parameter of the thickness reduction effect. It can be seen that, in general, ΔT increases with dose to a certain level and then tends to saturate in a clearly non-linear fashion. This non-linearity tells that there are other factors involved beyond dose alone.

More specifically, if comparing the trend lines for the initial film thickness of 31 nm, 63 nm and 131 nm at 3 keV exposure, it is obvious that with the same dose and energy, thicker film exhibits a higher ΔT. Further, by taking the derivative of

the trend lines, I found that the slopes of tangent lines increase with increasing the initial film thickness T_0, which suggests that effect of dose is enhanced by T_0. More evidence is presented in section 4.5 Initial Film Thickness Dependency on page 44.

Meanwhile, all fittings in Figure 4.2 are logarithmic except for 1 keV, in which case the fitting is better described by linear dependence. By comparing the trend line of initial thickness 63 nm at 1 keV with the trend line of initial thickness 63 nm at 3 keV, I observed that the trend line of 1 keV does not show the tendency of saturation within the given dose regime, whereas the trend line of 3 keV has the tendency to saturate. This may suggest that at lower energies, it would take relatively higher equivalent doses before saturation happens in comparison with higher energies. Also, when the dose increased from 33 to 66 μC/cm^2 (see also Table 4.1) in the trend line of 1 keV, ΔT increased from 2.9 to 5.5 nm, which corresponds to an increase of 0.079 nm per 1 μC/cm^2. On the other hand, in the trend line of 3 keV, when the dose increased from 100 to 200 μC/cm^2, ΔT increased from 6 to 10.8 nm, which corresponds to an increase of only 0.048 nm per 1 μC/cm^2. This shows that in lower energy regimes, the same increment of dose has greater impact on ΔT in comparison with similar increment of dose in higher energy regimes. This may also suggest that under lower energies, resist has a higher tolerance to high doses before cross-linking becomes significant, and thus greater ΔT can be achieved. Both observations above also support the argument that lower exposure energy is important in this developer-free process.

Interestingly, the trend line for an initial thickness T_0 = 31 nm and 3 keV exposure looks linear, but flat. Notice that, in this case, ΔT does not increase significantly with increasing dose. This is possibly because the penetration depth of 3 keV electrons is greater than the film thickness, which is 31 nm. Consequently, more energy is deposited into the substrate instead of the resist resulting in less interactions between electrons and the resist.

At last, I have also investigated the effect of multiple-passes, which is a process giving higher doses by exposing the same area multiple times rather than a single time. For example, a 400 $\mu C/cm^2$ dose is achieved by exposing the same area 4 times at 100 $\mu C/cm^2$. It can be seen that the result of multi-pass is the same as that of single exposure.

As for the etch efficiency η, in general, it decreases with decreasing dose. Comparing the trend line of 31 nm, 63 nm and 131 nm initial film thicknesses at 3 keV exposures, it can be observed that with the same dose and energy, thicker resist exhibits higherr η and the slopes of tangent lines also increase with increasing T_0. By comparing the trend lines of 63 nm initial film thickness at 1 and 3 keV exposures, I found that 1 keV always has a higher η value. This result, again, confirms that lower energy is more efficient for thickness reduction. The result of multiple-pass is also the same as for single exposure.

Finally, although not shown here, from all the AFM results obtained up to this stage, I noticed that higher doses produced a smoother surface.

4.4 Energy Dependency

To study energy dependency, a series of samples were exposed at various energies with the doses scaled proportionally to the energy to account for the normal variation in sensitivity [38, 77]. The detailed experimental conditions and numerical results are given in Table 4.2. Plots of ΔT vs. energy and η vs. energy are given in Figure 4.4 and Figure 4.5 respectively. Initial film thickness is denoted as T_0. The doses in this experiment are scaled linearly with energy with the reference condition being the dose at 1 keV. The resulting doses are referred to as the base doses, and the corresponding dose factors are equal to 1 for all energies.

Table 4.2 Experimental conditions and numerical results for energy dependency of ΔT and η

T_0 (nm)	Aperture (μm)	Energy (keV)	Dose (μC/cm^2)	Dose Factor*	ΔT (nm)	η (mm^3/C)
		1	73.3		6.1	8.3
		5	366.5		11.6	3.2
62±1	10	10	733	1	9.5	1.3
		20	1466		8.1	0.6
		30	2199		8.9	0.4

*The doses in this experiment are scaled linearly with energy with the reference condition being the dose at 1 keV. Therefore, the dose factor is 1 for all the energies.

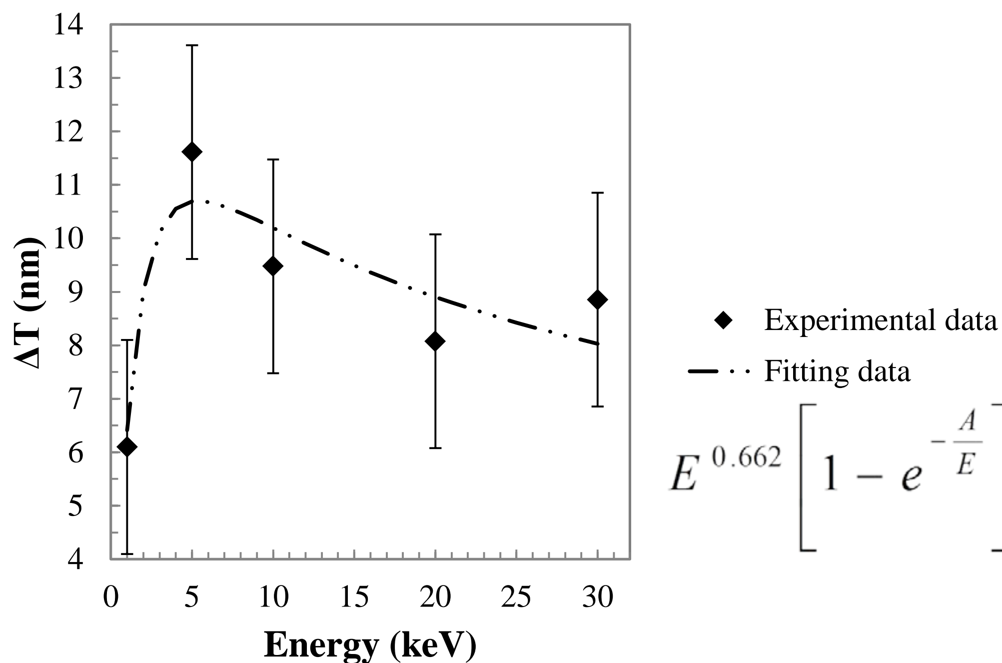

Figure 4.4 Energy dependency of ΔT. Sample was 62±1 nm 950k PMMA on Si, exposed at doses proportional to energy, no development. Base dose = 73.3 μC/cm^2 at 1 keV. In the fit formula, α = 0.66 and A = 4.17 eV. The error of AFM experimental data points is ±2 nm.

The results were obtained at constant dose factor. Therefore, higher energy corresponds to proportionately higher dose, reflecting the lowered sensitivity. The ΔT first increases dramatically from 1 keV to about 5 keV and then decreases with increasing energy. Clearly, at lower energies, the thickness reduction mechanism is very efficient and ΔT increases strongly with dose. However, at higher energies, less absorption occurs in the resist and most of the electrons penetrate deeply into the substrate, thereby reducing the impact of the beam current.

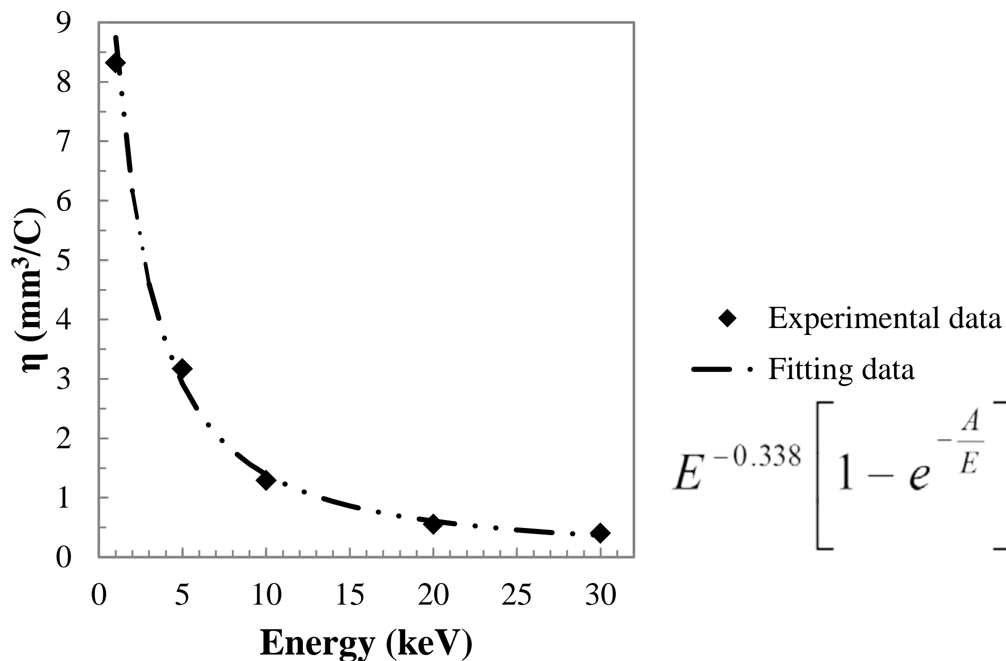

Figure 4.5 Energy dependency of η. Sample was 62±1 nm 950k PMMA on Si, exposed at doses proportional to energy, no development. Base dose = 73.3 μC/cm^2 at 1 keV. In the fit formula, α = 0.66 and A = 4.17 eV.

The etch efficiency, however, showed a very smooth and monotonic decrease with energy. The decrease in etch efficiency is very significant from 1 keV to about 5 keV reflecting clearly the importance of low energy regimes for thickness reduction.

Also included in these plots is a semi-empirical formula to fit the experimental results. The form stems from the probability of an inelastic collision occurring within the resist per electron ($1 - e^{-N\sigma t}$), where σ, ~ 1/E, is the inelastic collision cross section and E is the energy[38, 77], multiplied by the dose dependence,

which from Figure 4.2 appears to be a power law with $\Delta T \sim (\text{dose})^{\alpha}$. Since in this experiment exposure dose is proportional to energy E, the resulting formula becomes $\Delta T \sim E^{\alpha} (1 - e^{-A/E})$, where the parameters were fitted experimentally. The fitting captures the overall behaviour for ΔT and is also quite accurate for η. This suggests that electron collisions and the resulting fragmentation into volatile components is the dominant factor for thickness reduction, rather than energy deposition which would favour a resist evaporation mechanism. Finally, the energy where ΔT peaked in Figure 4.6 may shift to a different value if different thickness film is used or a different set of doses is applied. The reason is that both parameters will affect the electron-resist interactions and consequently alter the results.

4.5 Initial Film Thickness Dependency

Finally, the effect of initial film thickness T_0 on ΔT was considered. The detailed experimental conditions and numerical results are given in Table 4.3. Plots of ΔT vs. T_0 and η vs. T_0 are given in Figure 4.6 and Figure 4.7 respectively. Initial film thickness is denoted as T_0.

Table 4.3 Experimental conditions and numerical results for initial film thickness dependency of ΔT and η

T_0 (nm)	Aperture (μm)	Energy (keV)	Dose (μC/cm^2)	Dose Factor*	ΔT (nm)	η (mm^3/C)
31	10	3	400	4	9.7	2.4
63					18	4.5
131	20				32.9	8.2
31	10	3	600	6	10.9	1.8
63					20	3.3
131	20				37.4	6.2

*Dose factor equals dose normalized to the base dose at each energy level.

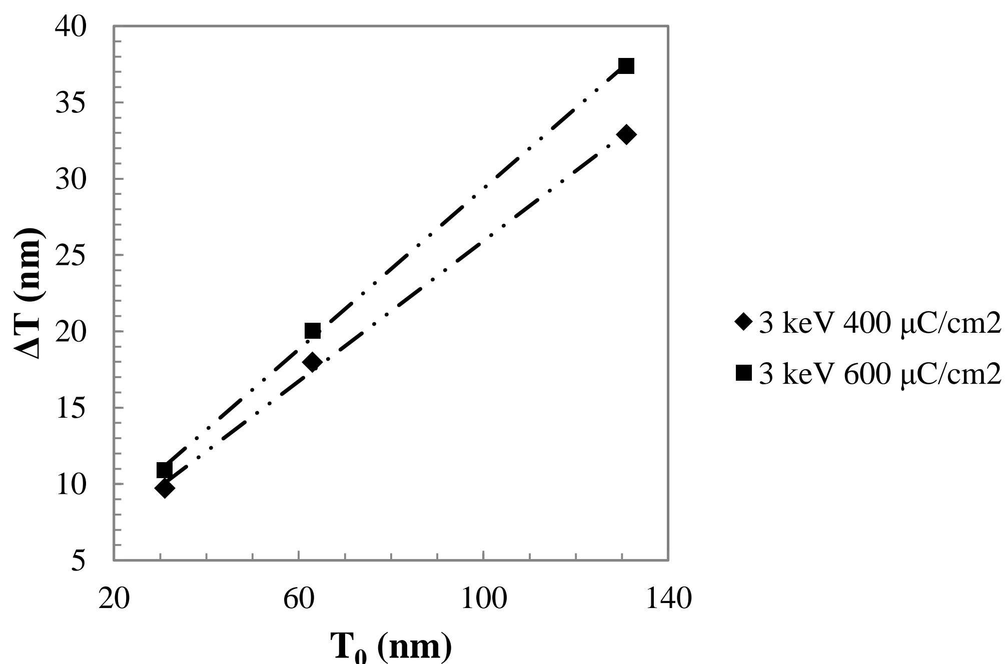

Figure 4.6 Initial film thickness dependencies of ΔT. Sample was 950k PMMA on Si, exposed at 3 keV, no development. Diamonds: 400 μC/cm^2; Squares: 600 μC/cm^2.

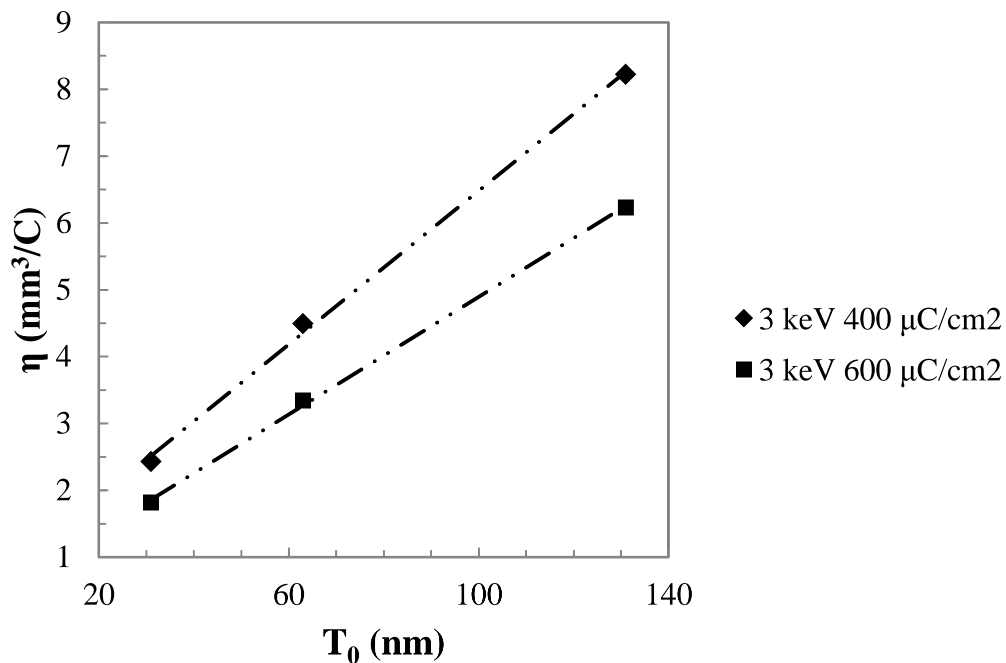

Figure 4.7 Initial film thickness dependencies of η. Sample was 950k PMMA on Si, exposed at 3 keV, no development. Diamonds: 400 μC/cm^2; Squares: 600 μC/cm^2.

As can be seen from the above results, both ΔT and η increase in proportion to T_0. If a surface dominated process such as electron beam evaporation were the main factor behind thickness reduction, then a strong T_0 dependence would not be expected. The linear behaviour evident in Figure 4.6 and Figure 4.7 supports a mechanism that depends on fragmentation throughout the volume such as production of volatile fragments.

From the experimental results and discussions above, one can see that the mechanism of thickness reduction is complex and exposure dose, energy and

initial film thickness have to be all considered simultaneously in order to achieve the optimum exposure conditions.

5 POST-EXPOSURE PROCESSING

The results above showed that exposure conditions can be optimized to increase the magnitude of thickness reduction at least up to 32%. However, it is unlikely that full clearance can be reached by exposure alone. Therefore, I proceeded with some post-processing techniques in an effort to reach total clearance without liquid development.

I considered two approaches, heating and RIE. As discussed above, the concept of heating is that it would drive off the remaining volatile fragments induced by electron beam exposure. For RIE, I simply wish to preserve the already existing height difference while reducing the thickness of exposed areas to zero. Under ideal circumstances, the fragmented exposed regions would be etched more quickly than the unexposed regions, thereby enhancing the height difference. However, this enhancement could be offset by a toughening in the exposed regions due to cross-linking by usage of high doses.

I included ZEP resist in these experiments because it provides better etch resistance yet sharing some similarities with PMMA. The resists used were standard 950k PMMA (1 - 2 %) from MicroChem Corp and ZEP 520A (ZEP:Anisole = 1:3) from Zeon Chemicals LP. PMMA samples were pre-baked before exposure at 150 °C for 5 min on hot plate. ZEP samples were pre-baked at 170 °C for 10 min on hot plate.

5.1 Heating

Following the electron beam exposure, some samples were baked on a hot plate. Detailed heating conditions and numerical results are given in Table 5.1 and Table 5.2 for PMMA and ZEP samples, respectively. Temperatures ranged from 47.5 to 290 °C. Temperature readings were taken from the thermocouple meter connected to the hot plate. Note that the glass transition temperatures for PMMA and ZEP are nominally 125 °C and 105 °C, respectively, although these may have been altered by conditions and processing.

5.1.1 Heating of PMMA samples

The experimental conditions and numerical results for PMMA heating dependency studies are given in Table 5.1. The heating influence on ΔT and η are plotted in Figure 5.1 and Figure 5.2, respectively.

Comparing the results of heating at 47.5 °C with those without heating, it can be seen that ΔT for 47.5 °C heating is slightly lower than that of un-heated sample at 400 $\mu C/cm^2$ dose. Then at dose 600 $\mu C/cm^2$, ΔT for 47.5 °C heating is slightly higher than that of un-heated sample. This can be likely explained as within experimental error. However, another possible explanation would be that due to moisture absorption. At 400 $\mu C/cm^2$ dose, fragmented PMMA due to electron beam induced chain scission absorbs more moisture than the PMMA exposed at 600 $\mu C/cm^2$ dose. Because at 600 $\mu C/cm^2$ dose, it is possible that cross-linking in

the resist due to the high dose just begins overtaking the chain scission. Consequently, localized resist densification and induced cross-linking reduced the absorption of moisture.

Table 5.1 Experimental conditions and numerical results for PMMA heating dependency studies

T_0 (nm)	Aperture (μm)	Energy (keV)	Dose (μC/cm^2)	Dose Factor*	Heating	ΔT (nm)	η (mm^3/C)
PMMA (Glass Transition Temperature is between 85 °C to 165 °C)							
31	10	3	400	4	No heating RT (23 °C)	9.5	2.4
			600	6		10.6	1.8
			800	8		11.8	1.3
			1,000	10		11.3	1.1
35	10	3	100	1	47.5 °C for 1 min	Not visible**	
			200	2		6.5	3.3
			400	4		8.1	2
			600	6		11.1	1.8
35	10	3	100	1	105 °C for 1 min	10.7	10.7
			200	2		23.3	11.7
			400	4		27.7	6.9
			600	6		21.1	3.5
31	10	3	400	4	282 °C for 30 min	19.5	4.9
			600	6		18.5	3.1
			800	8		17.5	2.2
			1,000	10		15.4	1.5
35	10	3	100	1	285 °C for 1 min	Clearance	
			200	2			
			400	4			
			600	6			
35	10	3	100	1	290 °C for 15 s	Clearance	
			200	2			
			400	4			
			600	6			

*Dose factor equals dose normalized to the base dose at each energy level.

**Exposed patterns could not be found by optical positioning microscope on the AFM.

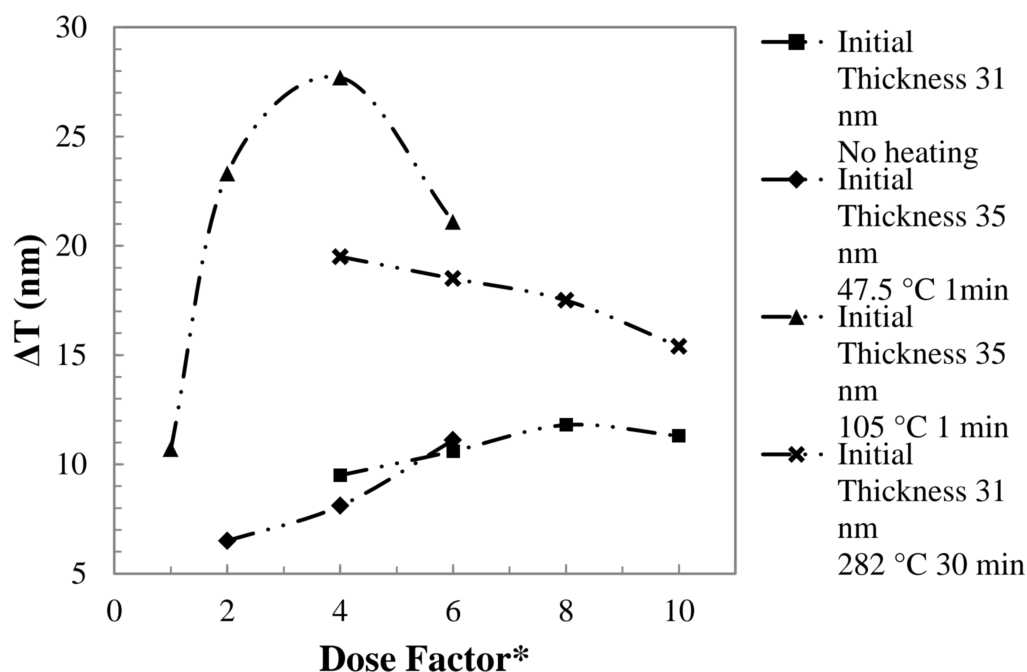

Figure 5.1 Heating influence on ΔT for PMMA. Sample was 950k PMMA on Si, no development. 3 keV Base dose = 100 μC/cm2. *Dose factor equals dose normalized to the base dose at each energy level.

The results for samples heated at 105 °C for 1 min with initial thickness T_0 = 35 nm showed that ΔT increased dramatically when dose increased from 100 to about 400 μC/cm^2 and then began to drop at higher doses. The dramatic increase may be attributed to the heating enhanced removal of small volatile products such as CO, CO2, CH3O and radical species [127]. The drop after 600 μC/cm^2 is presumably the result of cross-linking in the polymer during exposure due to increased dose, making the exposed region more stable because an increase in T_g. It is noteworthy that total clearance was almost achieved at the dose of 400 μC/cm^2.

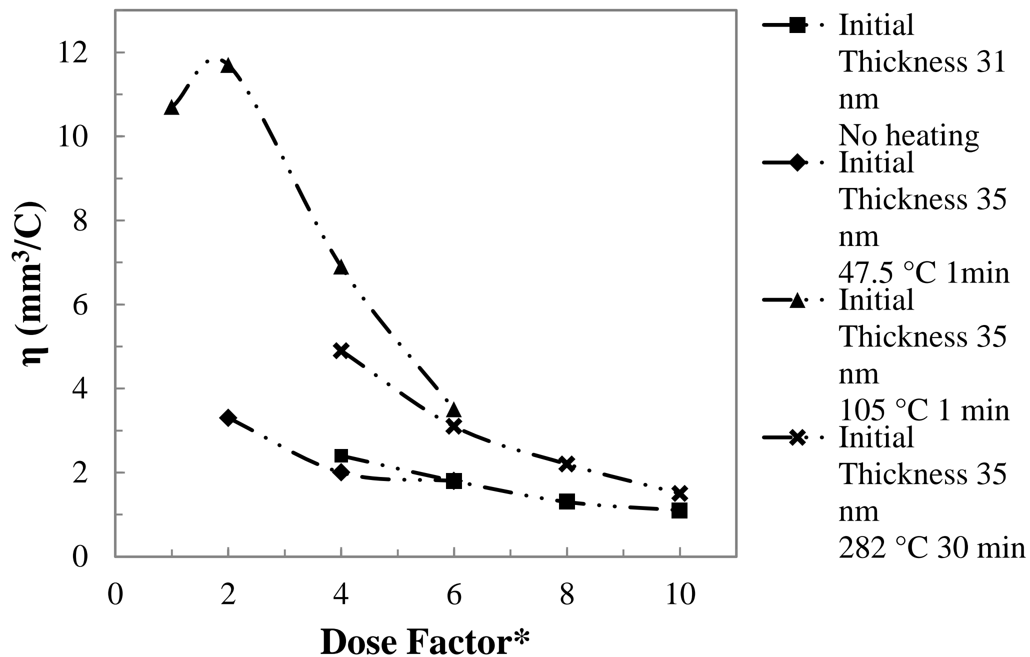

Figure 5.2 Heating influence on η in PMMA. Sample was 950k PMMA on Si, no development. 3 keV Base dose = 100 μC/cm^2. *Dose factor equals dose normalized to the base dose at each energy level.

When the temperature increased even higher to 282 °C with extended baking time, heating was not as effective in increasing ΔT as it was at 105 °C. It is obvious that ΔT is falling when dose increases under this heating condition. However, there are several interesting results which should be noted, as shown in Figure 5.3(e-f).

First, clearance has been achieved for the partially exposed areas surrounding the 1 μm^2 squares as shown in Figure 5.3(e-f). Second, inside the fully exposed 1 μm^2 regions, square islands with non-zero height began to emerge as shown in

Figure 5.3(e-f). These square islands are 5 to 6 nm in height and presumably arise as the result of cross-linking or carbonization of PMMA [136]. However, note that such island formation was also observed for 400 μC/cm^2 dose, although it was not obvious. Third, from this temperature onwards, the thickness of exposed and partially exposed PMMA was reduced while the thickness of un-exposed PMMA was increased. Examples are shown in Figure 5.4.

The sample in Figure 5.4 is a PMMA sample with initial thickness T_0 = 35 nm, exposed at 3 keV energy with the doses of (a) 100 μC/cm^2 ; (b) 200 μC/cm^2 ; (c) 400 μC/cm^2 ; (d) 600 μC/cm^2 ; and heated at 290 °C for 15 s. In the figure, it can be observed that the thickness of the lines/walls surrounding the 1 μm^2 squares and connecting the brighter spots/pillars decreases with increasing dose. On the other hand, the thickness of the bright spots/pillars increases with increasing dose. Even more surprisingly, the height of these bright spots/pillars is more than 50 nm, significantly exceeding the initial thickness T_0 (35 nm). This is a phenomenon which still needs to be understood. A hypothesis is that

> *"due to electron scattering, there is a gradient in molecular weight distribution as a function of distance from the exposed regions. Therefore there is a gradient of polymer glass transition temperatures as a function of position as well."* [55]

According to this theory, there should be also a gradient of molecular mobility as a function of distance from the exposed regions when heated. As the volatile

products evaporate and leave un-filled space, it may change the surface tension and the material may redistribute.

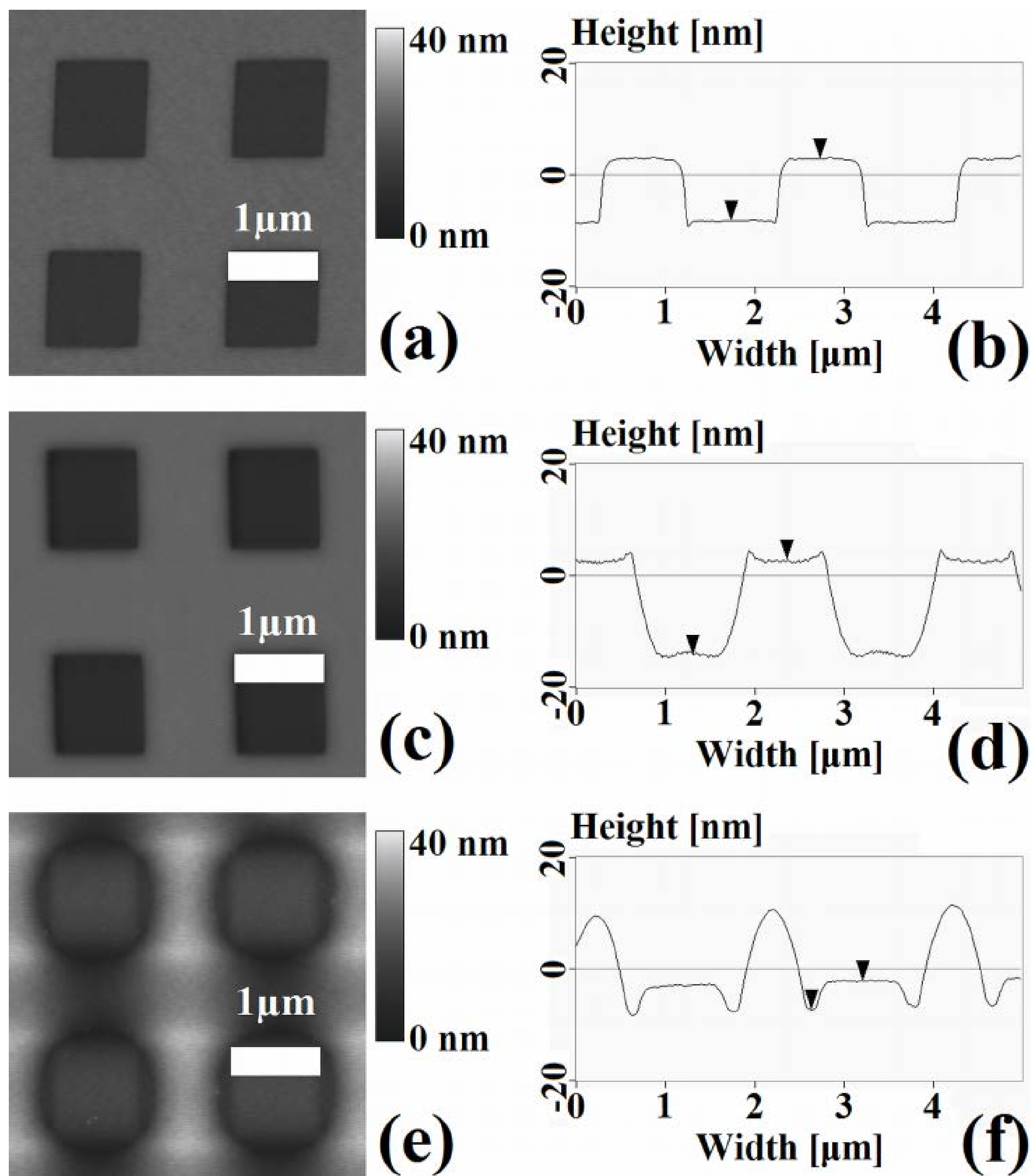

Figure 5.3 Comparison for no heating vs. heating. All samples were 950k PMMA on Si, exposed at 3 keV. Top view and cross-section view, respectively. (a-b) T_0 = 31 nm, 1000 µC/cm^2, no heating. ΔT = 11 nm. (c-d) T_0 = 35 nm, 600 µC/cm^2, 105 °C for 1 min. ΔT = 21 nm. (e-f) T_0 = 31 nm, 1000 µC/cm^2, 282 °C for 30 min. ΔT = 15 nm. Squares in the center are 5-6 nm in height.

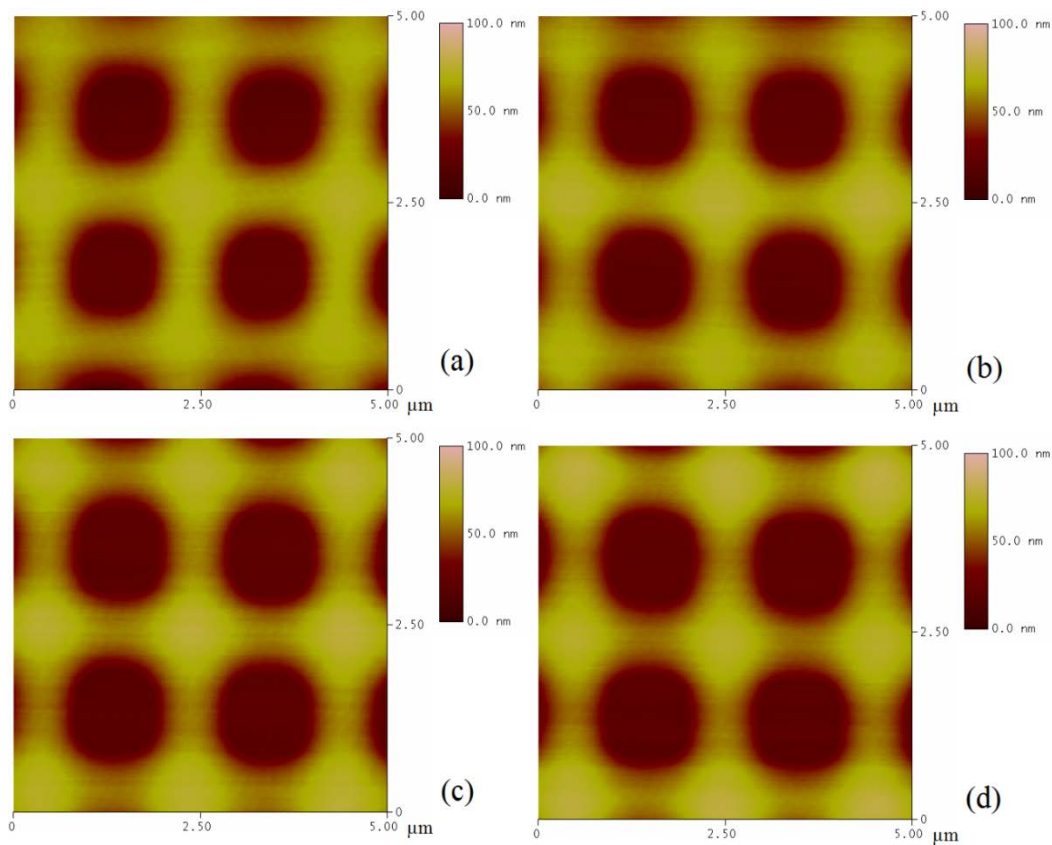

Figure 5.4 Thickness reduction and shape distortion under heating. 950k PMMA samples with initial film thickness T_0 = 35 nm, exposed at 3 keV, (a) 100 µC/cm^2 ; (b) 200 µC/cm^2 ; (c) 400 µC/cm^2 ; (d) 600 µC/cm^2 ; and heated at 290 °C for 15 s.

As for the origin of the over 50 nm pillars, it is possible that the heating induced some chemical conversion in the PMMA and a lower density material is formed. It is also possible that due to the surface tension of the material, the material is redistributed during the heating. Finally, total clearance was achieved for this sample at all doses applied and no obvious island formation was observed.

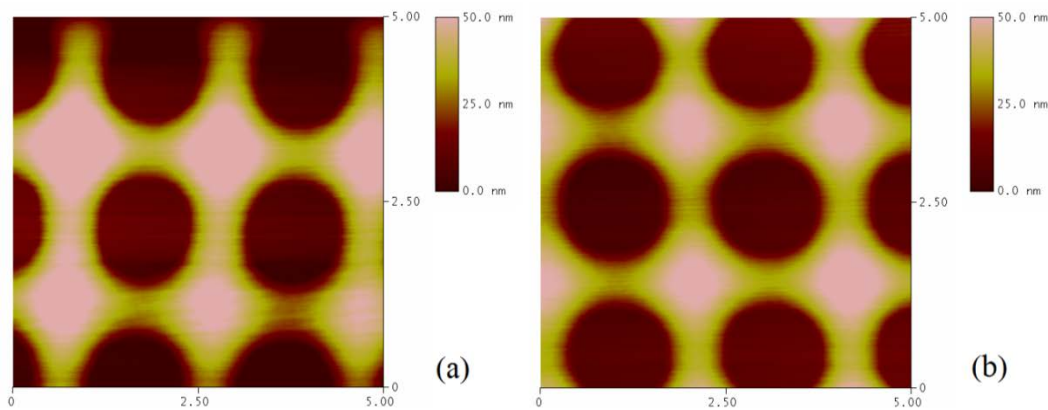

Figure 5.5 Effect of heating time. PMMA sample with T_0 = 35 nm, exposed at 3 keV, both at 400 μC/cm^2, heated at 285 °C for (a) 1min ; (b) 5 min.

Figure 5.5 illustrates the effect of heating time. The effect of heating time is relatively simple. With longer heating times, the enhancement of thickness reduction is more pronounced. However, the distortion induced by resist reflow becomes more severe too.

One concern of heating, especially at very high temperatures, is the reflow and distortion of the pattern as demonstrated in Figure 5.3. Figure 5.3(a-b) shows the profile for exposed but unheated PMMA. Although clearance was not reached, the thickness reduction was more than 33% of the initial film thickness. Figure 5.3(c-d) shows the result after heating at 105 °C for 1 minute. Note that the dose of Figure 5.3(c-d) was 600 μC/cm^2, which resulted in ΔT of 21 nm, about 60% of the initial film thickness (35 nm). Some reflow induced distortion began to develop but still remained moderate. Figure 5.3(e-f) shows the result after annealing at 282 °C for 30 min. The distortion due to the reflow is clear. Also, as

mentioned above, clearance was achieved for the partially exposed areas around the perimeter of the exposed squares, where the height difference is around 31 nm and 5-6 nm tall 1 μm^2 squares arose at the exposed sites, which may be due to the cross-linking or carbonization of PMMA [136] as a result of a long, high temperature baking. In comparison with the unheated sample shown in Figure 5.3(a-b), these two samples were exposed under exactly the same conditions. However, no island formation was observed for unheated sample. This suggests that heating could change the positive or negative behaviour of PMMA even when exposed under the same conditions. Further, it may imply that heating shifted the dose regime which determines the positive or negative behaviour to lower doses.

Up to this point, it is certain that heating is more effective in the lower dose regimes if a positive-tone PMMA process is employed. In Figure 5.6 and Figure 5.7 below, a comparison is made in order to determine the optimum dose for heating under the selected conditions. Two selected exposure doses, 400 and 600 $\mu C/cm^2$, are compared.

By observing the plots, it is clear that the dose of 400 $\mu C/cm^2$ gives better results than 600 $\mu C/cm^2$. Although at lower temperature, 600 $\mu C/cm^2$ dose has higher ΔT and η, lower temperature is not the most efficient regime for these heating experiments.

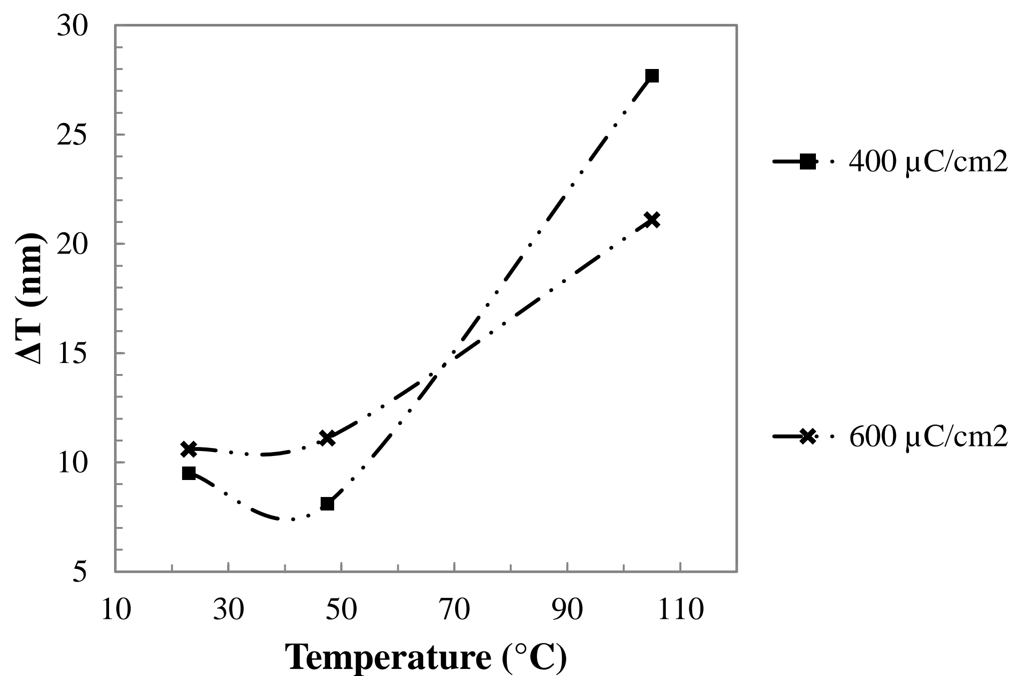

Figure 5.6 Optimum exposure dose when heating for ΔT. Sample was 950k PMMA on Si, no development. 3 keV Base dose = 100 μC/cm^2, heating time was 1 min for both samples. The temperature for unheated sample was presumed to be 23 °C.

However, taking the distortion induced by high temperature into consideration, the optimum temperature to heat PMMA samples may be close to 105 °C. As for heating time, shorter heating time will result in less distortion but also less enhancement of the thickness reduction.

Finally, lift-off has been attempted for un-heated and heated PMMA samples. The results showed that due to the carbonization or other alternation of the resist structure, further post-processing steps are required for lift-off to be successful.

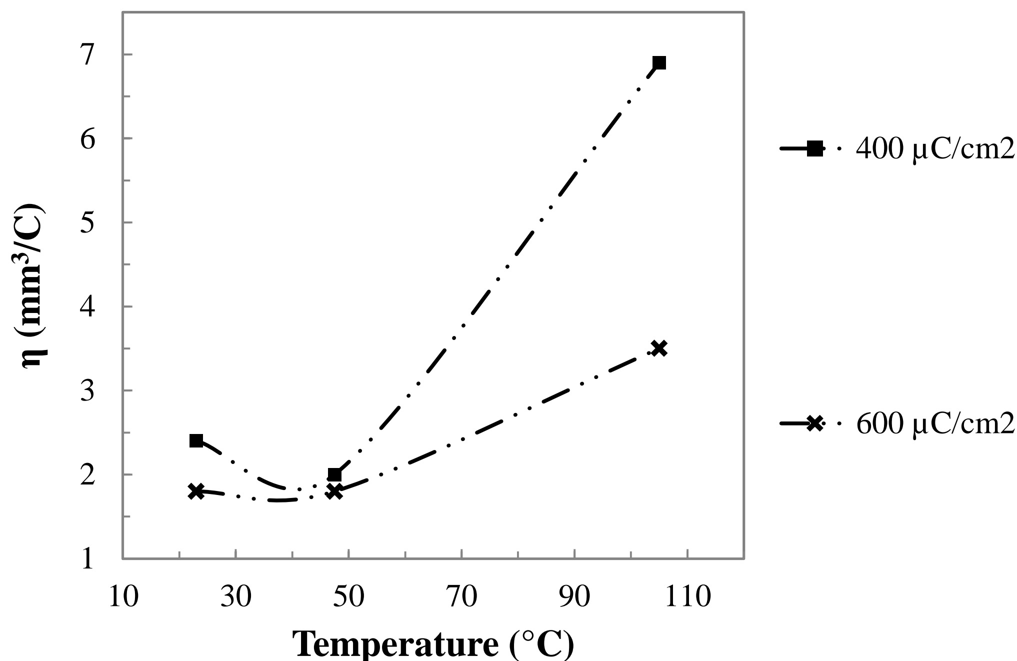

Figure 5.7 Optimum exposure dose in heating for η. Sample was 950k PMMA on Si, no development. 3 keV Base dose = 100 μC/cm^2 heating time was 1 min for both samples. The temperature for unheated sample was presumed to be 23 °C.

5.1.2 Heating of ZEP samples

Detailed heating conditions and numerical results of ZEP are given in Table 5.2. Plots of ΔT vs. dose and η vs. dose are shown in Figure 5.8 and Figure 5.9, respectively. Due to the higher sensitivity of ZEP, the doses of ZEP samples were scaled 4 times lower than the doses applied to PMMA for good comparison. Therefore, since the base for PMMA at 3 keV was 100 μC/cm^2, the base dose for ZEP at 3 keV was 25 μC/cm^2.

Table 5.2 Experimental conditions and numerical results for ZEP heating dependency studies

T_0 (nm)	Aperture (μm)	Energy (keV)	Dose (μC/cm^2)	Dose Factor*	Heating	ΔT (nm)	η (mm^3/C)
ZEP (Glass Transition Temperature is 105 °C)							
78	10	3	50	2	No heating	4	7.9
			100	4		6	6
			150	6		8.2	5.5
			200	8		10.2	5.1
78	10	3	50	2	75 °C for 30s	4	7.9
			100	4		10.6	10.6
			150	6		18.2	12.1
			200	8		20.8	10.4
78	10	3	50	2	100 °C for 1min	18.9	37.8
			100	4		37.9	37.9
			150	6		42	28
			200	8		44	22
78	10	3	50	2	290 °C for 15s	All patterns gone	
			100	4			
			150	6			
			200	8			

*Dose factor equals dose normalized to the base dose at each energy level.

First of all, the results of the unheated ZEP sample have confirmed that ZEP also exhibits thickness reduction after electron beam exposure. Comparing to PMMA, ZEP has a lower percentage of thickness reduction relative to initial film thickness T_0. With a dose factor of 8 at 3 keV, ΔT of unheated ZEP sample is 13% of T_0, whereas this value for unheated PMMA sample is more than 30% in most cases. This difference is explicable since less volatile products are produced by the scission of ZEP when exposed by electrons, more specifically due to the existence

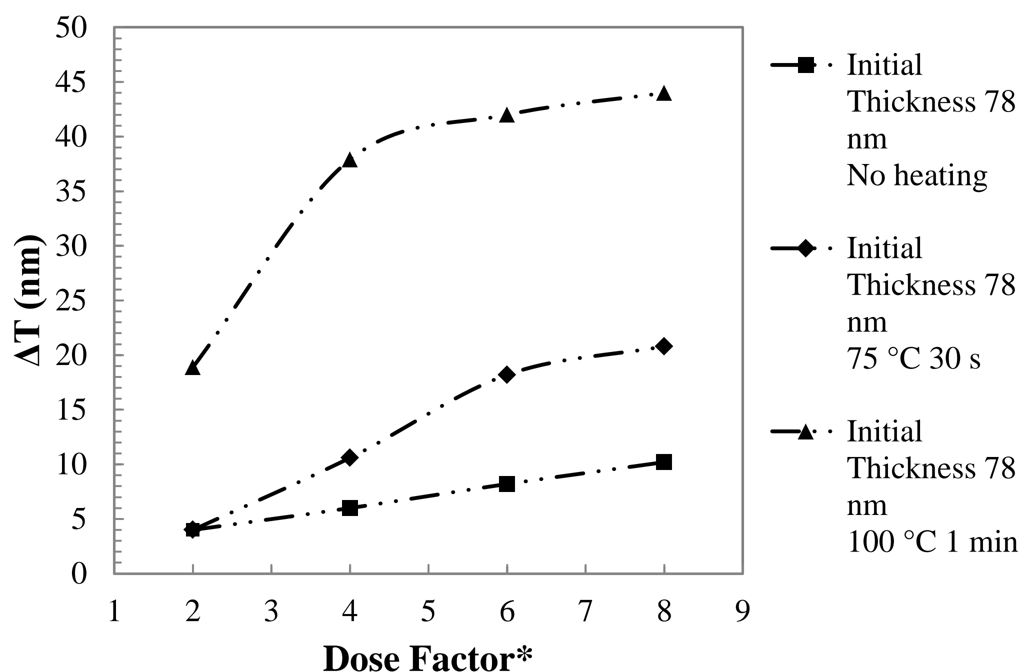

Figure 5.8 Heating influence on ΔT in ZEP. Sample was ZEP 520A on Si, no development. 3 keV Base dose = 25 μC/cm^2. *Dose factor equals dose normalized to the base dose at each energy level.

of α-methylstyrene in ZEP. Nonetheless, ZEP samples also demonstrated the effectiveness of heating, particularly at 100 °C.

Also, no drop of ΔT after dose factor 4 is observed at 100 °C heating for ZEP while there is a significant drop of ΔT at 105 °C heating for PMMA. This is probably because ZEP is more difficult to cross-link. This property suggests that higher doses can be applied to ZEP to achieve more substantial thickness reduction. It also seems that the trend of ΔT for ZEP is quite consistent under heating. After dose factor of 4, the curve of 75 °C and the curve of 105 °C seem

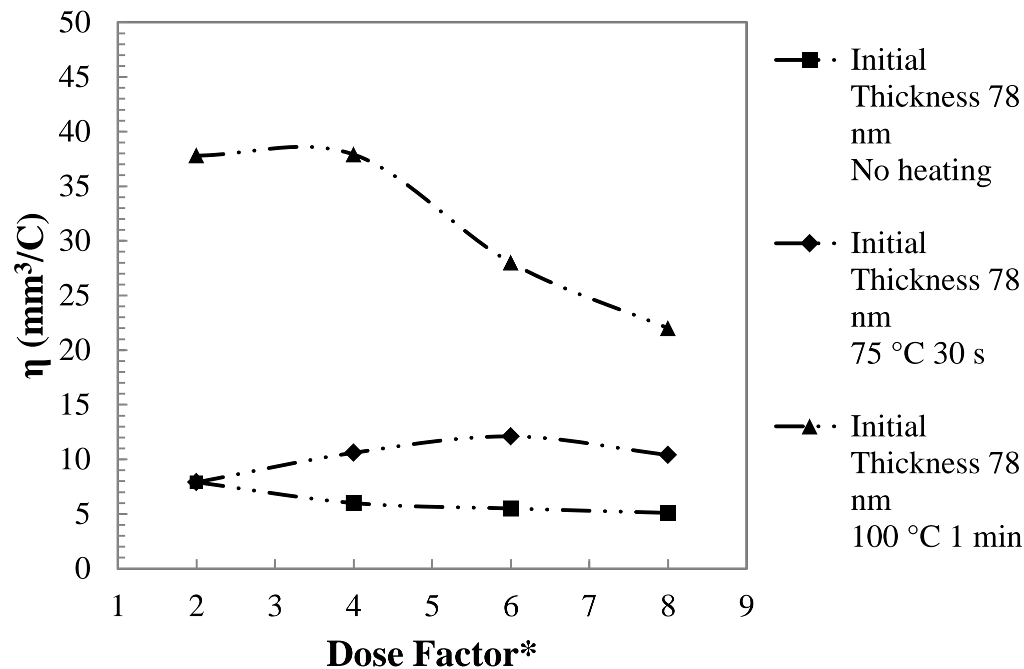

Figure 5.9 Heating influence on η in ZEP. Sample was ZEP 520A on Si, no development. 3 keV Base dose = 25 μC/cm^2. *Dose factor equals dose normalized to the base dose at each energy level.

to have a constant difference between them. This may suggest a linear temperature dependence of ΔT. However, under the heating conditions of 290 °C for 15s, all patterns were gone in ZEP, whereas for PMMA samples, the patterns still existed after being heated under the same conditions. This implies that ZEP is more sensitive, or in other words, less resistant to the effect of heating.

To conclude, it should be noted that the optimum temperature may be close to the glass transition temperature of the resist. However, this temperature may vary

depending on the molecular weight dispersity of the resist, the distribution of molecular weight, thickness of the film, and the material of the substrate.

5.2 Reactive Ion Etching

In addition to heating, I have also explored the potential of RIE to extend the thickness reduction effect. Two kinds of RIE processes have been tested. A normal RIE process at room temperature and an inductively coupled plasma RIE at −110 °C. The normal RIE process was performed with a Trion Phantom RIE system. The cryo-etch process was carried out by an Oxford Plasmalab System 100 - ICP 180.

5.2.1 Normal RIE process

5.2.1.1 Preliminary RIE tests for both PMMA & ZEP samples

The RIE study started with two preliminary RIE tests for PMMA and ZEP. The experimental conditions and numerical results are given in Table 5.3 and Table 5.4. T_t is the bulk resist thickness after RIE.

For both PMMA and ZEP samples, minor enhancement has been observed. The enhancement of PMMA samples seems to be greater than that of ZEP samples. However, note that the T_0 of PMMA RIE sample is 4 nm greater than the T_0 of its reference sample. Therefore, the value of ΔT before RIE should be slightly greater than the referencing value. Hence, the actual ΔT after RIE value may be lower than the reported one. Meanwhile, the thickness of bulk resist was not

measured after RIE, so it is hard to quantify and compare the results in a percentage way (e.g. what is the enhancement in percentage of the thickness reduction of bulk resist). Nevertheless, even without enhancement, if only the existing ΔT before RIE could be maintained during and after RIE while the exposed resist were etched to clearance, the RIE process would still be useful.

Table 5.3 Experimental conditions and numerical results of preliminary RIE tests for PMMA samples

Parameter	Units	Sample 1		Sample 2	
T_0	(nm)	31		35	
Aperture	(μm)	10		10	
Energy	(keV)	3		3	
Dose	(μC/cm^2)	400	600	400	600
Dose Factor*		4	6	4	6
ΔT before RIE	(nm)	9.5	10.6	9.5**	10.6**
Pressure	mTorr			5	
ICP power	W			N/A	
RF power	W			0	
Gase & Flow Ratio	sccm			O_2 = 20	
Time	s	N/A		120	
Temperature	°C			RT	
T_t	(nm)			N/A	
ΔT after RIE	(nm)			11.1	11.4
Enhancement	(nm)			1.6	0.8

*Dose factor equals dose normalized to the base dose at each energy level.

**Values are taken from the left sample.

Table 5.4 Experimental conditions and numerical results of preliminary RIE tests for ZEP samples

Parameter	Units	Sample 1				Sample 2			
T_0	(nm)	78				78			
Aperture	(µm)	10				10			
Energy	(keV)	3				3			
Dose	(µC/cm^2)	50	100	150	200	50	100	150	200
Dose Factor*		2	4	6	8	2	4	6	8
ΔT before RIE	(nm)	4	6	8.2	10.2	4**	6**	8.2**	10.2**
Pressure	mTorr					5			
ICP power	W					N/A			
RF power	W					0			
Gase & Flow Ratio	sccm					$O_2 = 20$			
Time	s	N/A				120			
Temperature	°C					RT			
T_t	(nm)					N/A			
ΔT after RIE	(nm)					3.9	6.5	8.8	10.7
Enhancement	(nm)					-0.1	0.5	0.6	0.5

*Dose factor equals dose normalized to the base dose at each energy level.

**Values are taken from the left sample.

5.2.1.2 Effect of exposure voltage on RIE (PMMA samples)

Next, I tested two more samples exposed at higher energies at 5 and 20 keV. The detailed experimental conditions and numerical results are given in Table 5.5. The results above showed two samples, with the same initial thickness T_0, and exposed at doses scaled linearly with energies. Therefore, the dose for 20 keV is 4 times higher than that of 5 keV. In this case, the bulk resist thickness T_t was measured after RIE. The 5 keV sample has a lower film thickness T_t after RIE than the 20 keV sample and yielded more enhancement. Also, the ΔT before RIE of the 5 keV sample is 3.5 nm greater than that of the 20 keV sample and the ΔT after RIE of the 5 keV sample is 3.7 nm greater than that of the 20 keV sample.

These observations suggest that lower energy is more efficient than higher energy for RIE process as well. The rest of the RIE experiments were conducted at 3 keV for consistency and easy comparison with other experiments and processing. Comparing to the preliminary tests, this experiment was at higher pressure and lower gas flow with 10 W of RF power, just the opposite condition to the preliminary tests. Yet, the RIE was still effective.

Table 5.5 Experimental conditions and numerical results of RIE for PMMA samples exposed at 5 and 20 keV

Parameter	Units	Sample 1	Sample 2
T_0	(nm)	61	61
Aperture	(µm)	10	10
Energy	(keV)	5	20
Dose	(µC/cm^2)	366.5	1466
Dose Factor*		1	1
ΔT before RIE	(nm)	11.6	8.1
Pressure	mTorr	100	100
ICP power	W	N/A	N/A
RF power	W	10	10
Gase & Flow Ratio	sccm	O_2 = 5	O_2 = 5
Time	s	60	60
Temperature	°C	RT	RT
T_t	(nm)	34.6	35.9
ΔT after RIE	(nm)	11.9	8.2
Enhancement	(nm)	0.3	0.1

*The doses in this experiment are scaled linearly with energy with the reference condition being the dose at 1 keV. Therefore, the dose factor is 1 for both energies.

5.2.1.3 Effect of RIE parameters (PMMA samples)

Following the above experiments, I examined the effects of various etching parameters and their combinations. So another set of experiments was completed. The detailed experimental conditions and numerical results can be found in Table

5.6. Since the primary goal of RIE processing was to reach clearance, maximum ΔT before RIE was desired and hence high dose was applied.

The results of this set of experiments were quite surprising. First, it seems that, at least under these particular conditions, etching parameters did not affect the ΔT after RIE. Second, ΔT reduced quite significantly. These two observations may suggest that the cross-linked or carbonized PMMA is very resistant to RIE and this resistance increases with the depth from initial film surface. Thus when certain depth is reached, the substance becomes so tough that the un-exposed resist is etched faster than exposed resist, thereby reducing the ΔT. The easy-to-etch layer before this occurs may be very thin. This would explain why the preliminary tests showed the enhancements but not these experiments. In addition to that, the doses of preliminary tests were not very high for PMMA and as already been discussed above, that ZEP has a higher tolerance to high dose before it begins to cross-link. Therefore, such a layer may be thicker in the preliminary tests. At last, the best result in this set of experiments is in the middle column where ΔT after RIE (13 nm) is about half of the bulk resist thickness after RIE T_t (27 nm). However, even if RIE would etch to clearance while maintaining the ΔT at 13 nm, such small height difference would be of only a limited applicability. For this reason, other methods were explored.

Table 5.6 Experimental conditions and numerical results of the effects of RIE conditions on PMMA samples

Parameter	Units	Sample 1	Sample 2	Sample 3
T_0	(nm)	106	106	106
Aperture	(μm)	20	20	20
Energy	(keV)	3	3	3
Dose	(μC/cm^2)	1000	1000	1000
Dose Factor*		10	10	10
ΔT before RIE	(nm)	38	38	38
Pressure	mTorr	50	50	5
ICP power	W	N/A	N/A	N/A
RF power	W	20	10	200
Gase & Flow Ratio	sccm	O_2 = 10	O_2 = 10	O_2 = 50
Time	s	30	120	5
T_t	(nm)	66	42	71.6
RF power	W	10	10	200
Gase & Flow Ratio	sccm	O_2 = 10	O_2 = 10	O_2 = 50
Time	s	45	23	5
T_t	(nm)	38	27	62.8
RF power	W	N/A	N/A	200
Gase & Flow Ratio	sccm			O_2 = 50
Time	s			5
T_t	(nm)			31.6
Temperature	°C	RT	RT	RT
ΔT after RIE	(nm)	13	13	13
Enhancement	(nm)	-25	-25	-25

*Dose factor equals dose normalized to the base dose at each energy level.

5.2.1.4 RIE for ZEP samples

I have also tried a different gas combination on a ZEP sample. The detailed experimental conditions and numerical results can be found in Table 5.7. A plot of dose dependency for this sample is also included in Figure 5.10.

Table 5.7 Experimental conditions and numerical results for CF_4:O_2 RIE test on ZEP sample

Parameter	Units	Sample 1			
T_0	(nm)	78			
Aperture	(μm)	10			
Energy	(keV)	3			
Dose	(μC/cm^2)	50	100	150	200
Factor*		2	4	6	8
ΔT before RIE	(nm)	4	6	8.2	10.2
Pressure	mTorr	50			
ICP power	W	N/A			
RF power	W	100			
Gase & Flow Ratio	sccm	CF_4:O_2 = 25:3			
Time	s	15			
Temperature	°C	RT			
T_t	(nm)	56.5			
ΔT after RIE	(nm)	2.7	5.1	7.6	9
Enhancement	(nm)	-1.3	-0.9	-0.6	-1.2

*Dose factor equals dose normalized to the base dose at each energy level.

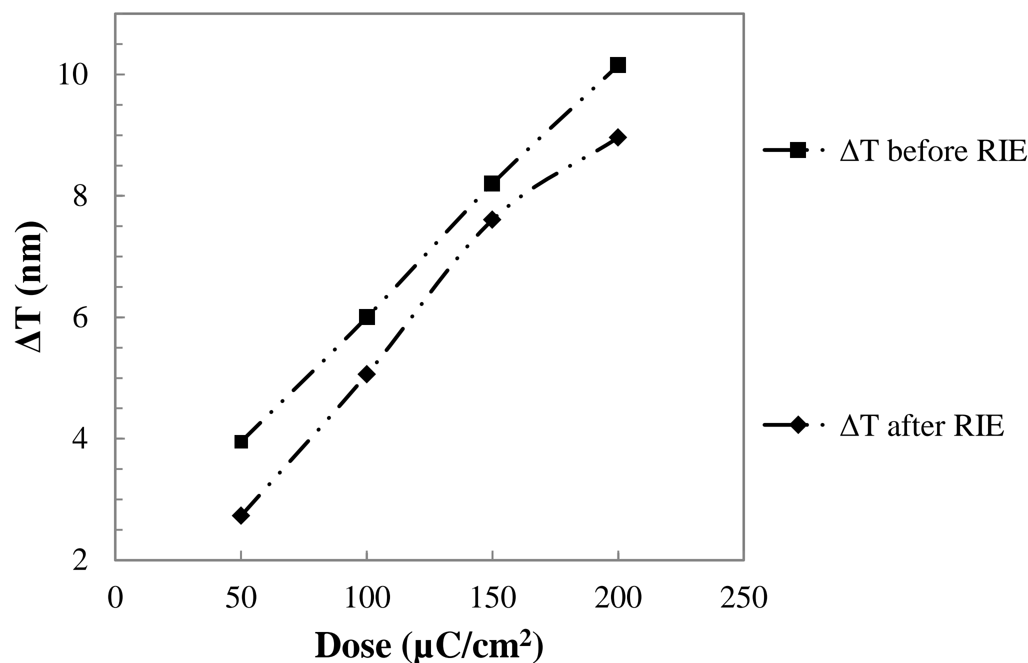

Figure 5.10 Dose dependency for CF_4:O_2 RIE test on ZEP sample.

It seems that the new combination of gases did not provide obvious advantages over the pure O_2 recipe. However, it is interesting to see that ΔT was better maintained with increasing dose up to about 150 $\mu C/cm^2$. This improvement suggests that there may be an optimum dose for RIE at given conditions.

5.2.2 Cryo-etch process

As the next step, I considered the cryo-etch process. As discussed in the above sections, there is a gradient of glass transition temperature as a function of distance from the exposure site. Due to this gradient, the T_g of the resist surrounding the exposed features is lower than the un-exposed resist but higher than the fully exposed resist. Therefore, when cooled to low temperature, the un-exposed resist and partially exposed resist would freeze faster and became harder than fully exposed resist. If etched under this condition, it may improve the etching preference to the exposed resist and better maintain the ΔT.

5.2.2.1 Cryo-etch for PMMA samples

The first cryo-etch experiment was carried out on a sample which was exposed under the same conditions as the samples etched by normal RIE presented in Table 5.6.

The detailed experimental conditions and numerical results are given in Table 5.8 below. I have also examined the morphology of resist after cryo-etch. The results are shown in Figure 5.11.

Table 5.8 Experimental conditions and numerical results of first cryo-etch on PMMA sample

Parameter	Units	Sample 1	Comment
T_0	(nm)	106	
Aperture	(μm)	20	
Energy	(keV)	3	
Dose	(μC/cm^2)	1000	
Dose Factor*		10	
ΔT before RIE	(nm)	38	
Pressure	mTorr	5	De-scum
ICP power	W	150	
RF power	W	20	
Gase & Flow Ratio	sccm	O_2 = 20	
Time	s	5	
Temperature	°C	−110	
Pressure	mTorr	7.5	Etching
ICP power	W	400	
RF power	W	6	
Gase & Flow Ratio	sccm	SF_6:O_2 = 45:10	
Time	s	15** × 4 = 60	
Temperature	°C	−110	
T_t	(nm)	34	
ΔT after RIE	(nm)	19.7	
Enhancement	(nm)	-18.3	

*Dose factor equals dose normalized to the base dose at each energy level.

** The sample was taken out for inspection of film thickness after each 15 s etch.

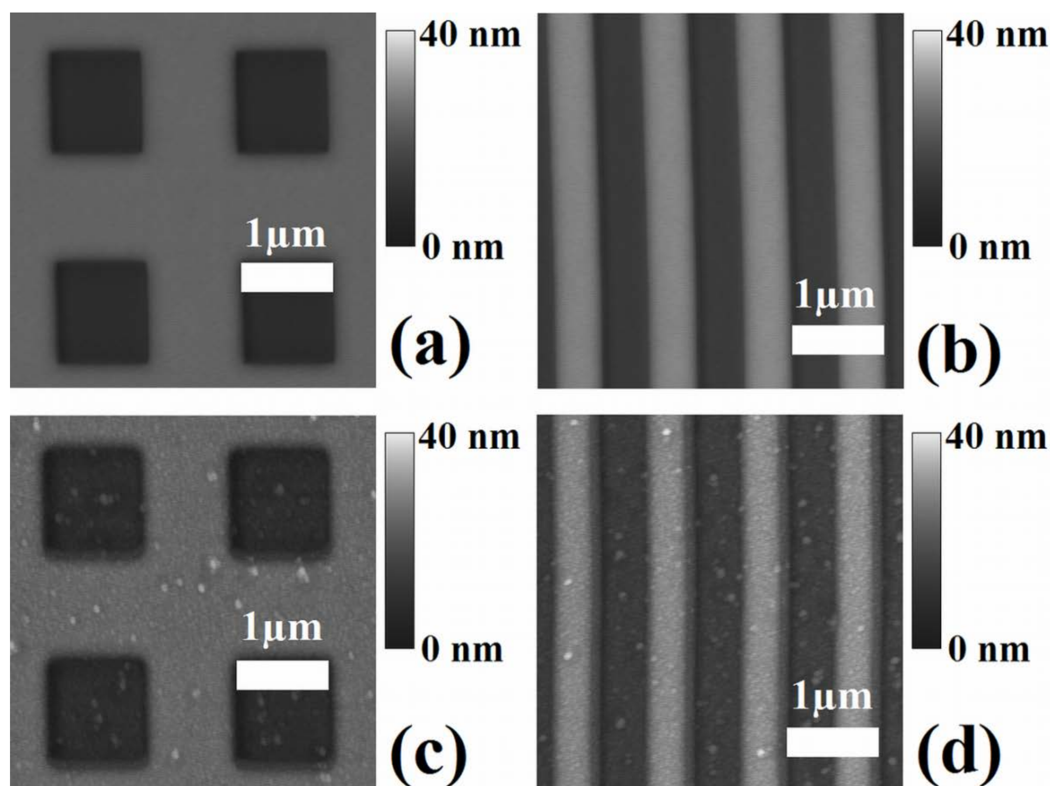

Figure 5.11 Morphology of resist after cryo-etch. 950k PMMA on Si, exposed at 3 keV, 1000 μC/cm$_2$, no development. 1 μm squares and 500 nm lines with 500 nm spacing, respectively. (a-b) Before ICPRIE, initial film thickness = 106 nm, ΔT = 38 nm. (c-d) After ICPRIE at -110 °C, de-scum at 5 mTorr, O_2 = 20 sccm, ICP = 150 W, RF = 20 W, 5 s, etching at 7.5 mTorr, SF_6:O_2 = 45:10 sccm, ICP = 400 W, RF = 6 W, 60 s, film thickness = 34 nm, ΔT = 20 nm.

Immediately after the exposure, the sample had a film thickness of 106 nm with ΔT = 38 nm. After the cryo-etch, film thickness was reduced to 34 nm with ΔT = 20 nm. Note that ΔT was reduced too. This means exposed region was etched slower than the unexposed region. As mentioned above, the reason could be that the exposed region was hardened by resist cross-linking. I also noticed that there were small pieces of PMMA re-deposited on the surface after RIE. A possible

solution would be to add another de-scum procedure after the etching is done. Although in my experiments, normal RIE process did not have this issue, I believe that cryo-etch is a better process than normal RIE. The major reason is that cryo-etch indeed preserved the ΔT better than the normal RIE process. It can be observed by comparing this cryo-etch sample with other normal RIE samples in Table 5.6. These samples were exposed under the same conditions (ΔT = 38 nm) but subjected to different RIE processes. For the samples which went through the normal RIE process, ΔT decreased to 13 nm; however, for the sample which went through the cryo-etch process, ΔT decreased to 20 nm.

5.2.2.2 Dose dependency during cryo-etch for PMMA samples

Since a dependency of dose during normal RIE for ZEP has been observed, another dose dependency study was conducted for the PMMA samples in the cryo-etch process. The detailed experimental conditions and numerical results are given in Table 5.9 below. The plots are shown in Figure 5.12. Also, recall the results of energy dependency study from Figure 4.4 in page 42. The ΔT peaked near 5 keV. Therefore, a comparison between 3 and 5 keV has been made in this study too.

The results showed that although cryo-etch did not enhance or preserve the ΔT, the ΔT increases with increasing dose up to about 400 μC/cm^2 and then decreases with the dose. This is consistent with the optimum heating dose value (see Figure 5.1), which may suggest that the molecular mechanisms of scission and/or cross-

linking in PMMA are dose dependent and undergo changes around 400 μC/cm^2 for 3 keV exposure, despite the difference in film thickness (35 nm for the sample in Figure 5.1 and 131 nm in this case).

Table 5.9 Experimental conditions and numerical results of dose dependency during cryo-etch for PMMA sample

Parameter	Units	Sample 1					Sample 2	Comment
T_0	(nm)	131					131	
Aperture	(μm)	20					20	
Energy	(keV)	3					5	
Dose	(μC/cm^2)	200	400	600	800	1000	1000	
Dose Factor*		2	4	6	8	10	6**	
ΔT before RIE	(nm)	20.6	32.9	37.4	39.7	41.7	38.1	
Temperature	°C	−110						
Pressure	mTorr	5						De-scum
ICP power	W	150						
RF power	W	20						
Gase & Flow Ratio	sccm	$O_2 = 20$						
Time	s	10						
Pressure	mTorr	7.5						Cryo-etch
ICP power	W	400						
RF power	W	6						
Gase & Flow Ratio	sccm	$SF_6:O_2 = 45:10$						
Time	s	10						
Pressure	mTorr	5						De-scum
ICP power	W	150						
RF power	W	20						
Gase & Flow Ratio	sccm	$O_2 = 20$						
Time	s	10						
Pressure	mTorr	7.5						Cryo-etch
ICP power	W	400						
RF power	W	6						
Gase & Flow Ratio	sccm	$SF_6:O_2 = 45:10$						
Time	s	30					30	
T_t	(nm)	37.6					40.6	
ΔT after RIE	(nm)	14.3	19	17.6	16.6	15.6	20.4	
Enhancement	(nm)	-6.3	-13.9	-19.8	-23.1	-26.1	-17.7	

*Dose factor equals dose normalized to the base dose at each energy level.

**Due to the higher energy, this dose is equivalent to 600 μC/cm^2 at 3 keV.

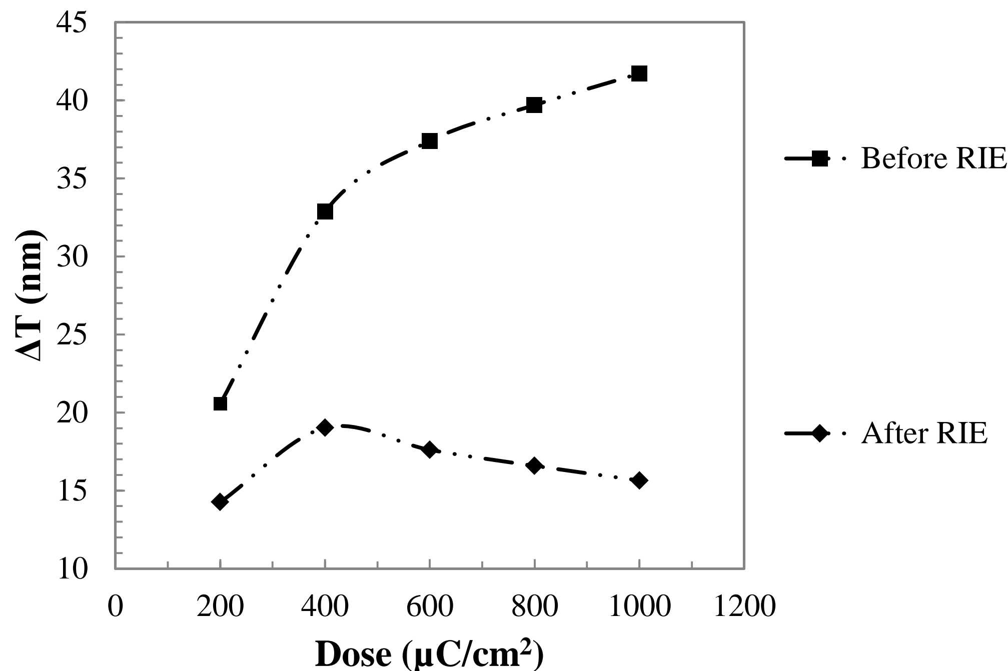

Figure 5.12 ICPRIE dose dependency for ΔT. Sample was 131 nm 950k PMMA on Si, exposed at 3 keV with no development. ICPRIE was performed at -110 °C, de-scum at 5 mTorr, O_2 = 20 sccm, ICP = 150 W, RF = 20 W, etching at 7.5 mTorr, SF_6:O_2 = 45:10 sccm, ICP = 400 W, RF = 6 W. The process comprised 10 s de-scum and 60 s etch followed by another 10 s de-scum and 30 s etch.

For this reason, it seems that lower dose regimes would be more effective in RIE too and the optimum dose at 3 keV may be close to 400 μC/cm^2 as well.

As for the optimum energy, the results of 5 keV is slightly better than that of 3 keV. This is also consistent with the conclusion of energy dependency studies (see Figure 4.4). However, as discussed in section 4.4 Energy Dependency, the optimum energy may change depending on the initial film thickness and doses applied.

5.2.2.3 Cryo-etch for ZEP samples

The same cryo-etch recipe has been applied to ZEP samples. Furthermore, I also investigated the effect of several short etches with equal duration versus a single etch with the duration equal to the sum of short etching durations. The detailed experimental conditions and numerical results are given in Table 5.10 below.

Table 5.10 Experimental conditions and numerical results of cryo-etch for ZEP samples and the effect of etching time interval

Parameter	Units	Sample 1	Sample 2	Comment
T_0	(nm)	78		
Aperture	(µm)	10		
Energy	(keV)	3		
Dose	(µC/cm^2)	200		
Dose Factor*		8		
ΔT before RIE	(nm)	10.2		
Temperature	°C	−110		
Pressure	mTorr	5		De-scum
ICP power	W	150		
RF power	W	20		
Gase & Flow Ratio	sccm	$O_2 = 20$		
Time	s	5	10	
Pressure	mTorr	7.5		Cryo-etch
ICP power	W	400		
RF power	W	6		
Gase & Flow Ratio	sccm	$SF_6:O_2 = 45:10$		
Time	s	15** × 3 = 45	45	
T_t	(nm)	24	34	
ΔT after RIE	(nm)	Not visible***	9.1	
Enhancement	(nm)	N/A	-1.052	

*Dose factor equals dose normalized to the base dose at each energy level.

** The sample was taken out for inspection of film thickness after each 15 s etch.

***The patterns could not be found by optical positioning microscope on the AFM.

The results above showed that there is a difference between several short etches versus a single long etch. Note that the de-scum time of the single long etch

sample is longer than the multiple short time etch sample. Therefore, more resist should be etched for the single long etch sample. However, even with this difference, it seems that several short etches still produced more resist thinning of the bulk film. More specifically, the bulk film thickness after etch (T_t) of multiple short etch sample is 24 nm, which is less than that of the single long etch sample (34 nm). A possible explanation is as follows. It normally takes about 5 s for a RIE system to stabilize to the set conditions. This process is known as tuning. When operated under the auto mode, each time etch begins, the system will spin the tuning capacitor around trying to find the optimal tune. Because of this repeating tuning process, overshoot may occur each time etch starts and hence produced more thickness reduction. This effect is not desired because it adds uncertainty to the experiments. To offset this effect, the system can be operated under the manual mode. In this mode, after the first tuning, the position of tuning capacitor will not change and it should be in its optimal position for the rest of experiments as long as the same recipe parameters are set from run to run.

Another observation from the above results is that the decrease of ΔT of ZEP samples after cryo-etch is less than that of PMMA samples. Considering that ZEP samples also yielded less enhancements in preliminary RIE tests, I believe the reason is that ZEP is overall more resistant to RIE than PMMA [85, 86]. This is a positive factor for RIE process because it can preserve ΔT better. However, ZEP also exhibits less thickness reduction after electron beam exposure, too. Therefore, there is a trade-off between the selection of PMMA and ZEP. PMMA

exhibits more thickness reduction after electron beam exposure but suffers from the decrease of ΔT during RIE. On the other hand, ZEP exhibits less thickness reduction after electron beam exposure but withstands the RIE and preserves ΔT better. PMMA is easily cross-linked by high doses whereas ZEP is more tolerant to high doses before cross-linking becomes significant. To conclude, although the work shown in this thesis focuses more on PMMA as it is an overall better understood resist, ZEP also has a potential to make this developer-free approach a better process and more investigations should be done to further realize its potential.

6 HIGH RESOLUTION TRIALS

In this chapter, a few experiments for achieving high resolution dense gratings are presented. The standard test structures used for the above experiments were relatively big (1 μm^2 squares) so that both AFM inspections and calculations can be easily done. However, I have managed to pattern dense high resolution gratings on both PMMA and ZEP samples without liquid development or post-exposure processing. A Hitachi S4800 was employed to inspect the samples.

6.1 Challenges during SEM imaging

A major problem during SEM is the resist damage due to SEM electrons. The patterns are being erased during SEM, which in fact exposes the patterns again while imaging. After zooming in and zooming out, the pattern was totally destroyed. I have tried coating the samples with Cr. Surprisingly, the contrast was reduced by coating, possibly because the metal layer evened out the patterns. I have also examined the effect of utilizing high exposure doses. It seems that high dose created deeper patterns that were still recognizable after imaging and the image looks sharper too. Also, I noticed that there are a few seconds for adjustments (focus and stigmation) before the patterns are totally destroyed. This is how the successful images are taken. However, due to the short time window for adjustments and the fact that the electron dose during SEM scales up with magnification and hence more damage to the pattern, higher magnification images

were not obtained. Lastly, most of the images shown in the following discussions were obtained without Cr coating unless otherwise noted.

6.2 70 nm half-pitch gratings

So far, 70 nm half-pitch gratings have been successfully pattern on both PMMA and ZEP resist. An example of the results is shown in Figure 6.1.

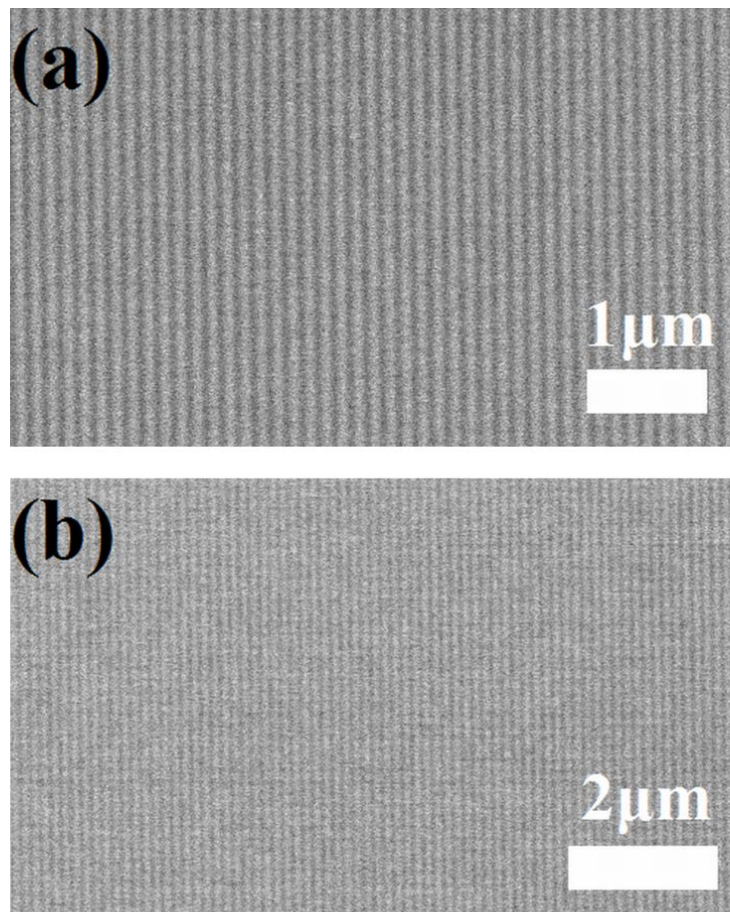

Figure 6.1 70 nm half-pitch gratings on PMMA and ZEP. SEM images of 70 nm half-pitch gratings exposed at 3 keV, 7.5 μm aperture, no development, on (a) 72 nm 950k PMMA on Si, ~ 600 μC/cm2 (b) 64 nm ZEP 520A on Si, ~ 100 μC/cm^2. The dose range of the PMMA sample was from 100 to 900 μC/cm^2 and the ZEP sample was from 25 to 225 μC/cm^2.

40 and 50 nm half-pitch gratings were achieved too. However, due to the imaging challenge, the quality of the images was not very persuasive. Thus the results are not included.

6.3 Developer-free vs. Liquid development

Finally, I made a comparison between liquid development and developer-free approach with ZEP samples. The results are shown in Figure 6.2

Developer-free **Liquid development**

50 nm lines with 250 nm spacing, E-Beam, 3 keV, 7.5 μm aperture

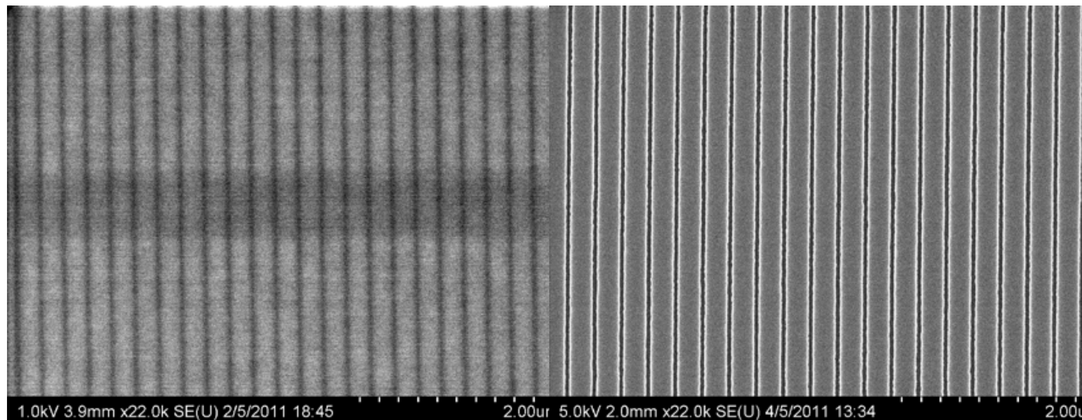

Developer-free:

- 64 nm ZEP 520A
- Area Dose = 200 μC/cm^2 (equivalent to Line Dose 40 pC/cm)
- No development
- Not coated with Cr

Liquid development:

- 61 nm ZEP 520A
- Line Dose = 40 pC/cm
- Developed in ZED N-50 for 30 s followed by 20 s rinse in MIBK
- Coated with Cr

Figure 6.2 Developer-free vs. Liquid development

It should be note that developer-free sample was not coated with Cr whereas the liquid development sample was coated with Cr. Hence the image contrast of liquid development sample is better. While the developer-free sample has likely not cleared down to the substrate, the contrast modulation observed does indicate that the thickness reduction is scalable to high resolution structures. Although the doses employed in the experiments prior to this chapter are generally higher than the doses required for conventional liquid development, it seems that for dense gratings, it is also possible to achieve considerable thickness reduction at comparable doses to conventional liquid development for the pattern to be visualized. For example, the samples from Figure 6.2 were exposed at equivalent doses though the unit was in area dose and line dose. In other words, the value of dose is the same if converting the area dose to line dose or vice versa. This suggests the possibility to utilize the developer-free approach at a lower dose regime that is closer to the conventional liquid development EBL process.

7 CONCLUSIONS & OUTLOOK

7.1 Conclusions

The purpose of this thesis work is to utilize the resist thickness reduction due to electron beam irradiation and investigate a patterning approach without the usage of liquid development. I have employed heating and RIE as post-exposure processes in order to increase thickness reduction and obtain pattern clearance. Even without any post-exposure processing, I have observed substantial thickness reduction up to 38% by electron beam irradiation. This reduction is likely due to the production of volatile fragments through the scission process in the resist. The thickness reduction induced by electron beam irradiation depends on exposure dose, beam energy, and initial film thickness. The doses required for this process are generally higher than typical exposure doses used in standard liquid development processes. Low exposure energy is particularly important to achieve thickness reduction. Post-exposure heating can increase the height difference and even achieve clearance; however, at the risk of pattern distortion. The effectiveness of post-exposure heating is likely due to the evaporation of less volatile fragments. There is an interaction between heating and optimum dose, probably because of cross-linking and carbonization. To date, 70 nm half-pitch gratings have been successful patterned on both PMMA and ZEP without liquid development. Further optimization of both exposure and post-processing is possible, with good prospect for a viable EBL patterning process that does not require liquid development.

7.2 Outlook

Presently, the developer-free EBL patterning is at an early stage research. Many parameters can be optimized in future experiments. Based on the observations made, I believe the exposure dose should be reduced to about 400 $\mu C/cm^2$ if 3 keV energy is used for optimum results. It would be helpful to further extend the modelling of energy dependencies with the ultimate goal to precisely predict the most efficient energy when other parameters vary.

It would be also interesting to heat thicker samples since thickness dependency of physicochemical properties of PMMA have been observed [132]. It is possible that thicker resist would perform better in the heating process. What also worth doing would be heating the samples in a vacuum ambient because lowered pressure may enhance the evaporation of volatile fragments.

As for the RIE conditions, at this stage, further study is needed to find out whether ion sputtering etch or reactive ion chemical etch should be the principal process during the RIE, as well as how to balance these two factors. Regarding the reduced etch preference to exposed resist during RIE, certainly further exploration in cryo-etch would be helpful. In the meantime, the alternative would be to try out a soft post-exposure bake before RIE. One can expect that the baking would harden the unexposed and partially exposed film so that their etch resistance is improved. Through co-optimization with the exposure conditions, I expect total pattern clearance could be achieved with RIE as well.

For the imaging challenge, it would be worthwhile to try tilted imaging because that would provide more contrast. Another alternative would be cleaving the sample in liquid nitrogen and imaging the cross-section of the pattern.

Another non-trivial factor in the overall process is the pre-exposure sample preparations. What kind of solvent the resist is prepared with and the residual solvent after pre-bake may also have an impact on the thickness reduction after electron beam exposure. Therefore, the effect of pre-bake conditions such as temperature and time should be studied and considered in the overall process.

Inspired by the research conducted by D. A. Czaplewski and L. E. Ocola [89], the applicability of second exposure after post-exposure processing may be explored.

It would also be interesting to investigate the viability of this developer-free approach to other electron beam resists such as HSQ. Because HSQ undergoes cross-linking when exposed by electron beam, it may exhibit thickness change too. Other research has shown that it is possible to thermally develop calixarene resist [131], which may imply that thermal development may work for HSQ as well.

Finally, because ion beam lithography has a number of similarities with EBL (such as ion beam induced chain scission in positive-tone resist and cross-linking in negative-tone resist) [137], and provides several advantages, for example a

high sensitivity [138], a developer-free resist processing may be extendable to this technology as well. The possibility of resist thinning by ion beam processing is well known [139] and worth a further exploration. Potentially this may lead to novel processing concepts building on a foreseeable convergence of lithographic and etching technologies.

8 REFERENCES

[1] Encyclopædia Britannica Online. Lithography. *2011*Available:

http://www.britannica.com/EBchecked/topic/343748/lithography.

[2] Chris Mack. Semiconductor lithography - the basic process. *2011*Available:

http://www.lithoguru.com/scientist/lithobasics.html.

[3] E. Reichmanis and A. E. Novembre, "Lithographic resist materials chemistry," in *Annual Review of Material Science*Anonymous Palo Alto, CA, United States: Publ by Annual Reviews Inc, 1993, pp. 11-43.

[4] H. N. G. King, "Electron beam lithography," *Microelectronics,* vol. 1, pp. 28-30, 11, 1967.

[5] A. N. KABANOV, G. A. MIKHAILOVSKII, N. I. PANTELEEV and I. P. SELEZNEV, "E-8 HIGH- VACUUM ELECTRON- BEAM APPARATUS," vol. 32, pp. 887-90, 1968.

[6] M.A.Mohammad, T. Fito, J. Chen, S. Buswell, M. Aktary, S.K. Dew, and M. Stepanova. "The interdependence of exposure and development conditions when optimizing low-energy EBL for nano-scale resolution," in *Lithography* (1st ed.), Michael Wang, Ed. 2010), Available:

http://sciyo.com/articles/show/title/theinterdependence-of-exposure-and-development-conditions-when-optimizing-low-energy-ebl-for-nanos?PHPSESSID=2s6gs1jtfkgkq5jio3hgpdups1.

[7] F. Robin. Electron-beam lithography applications at ETH zurich. *Raith application note(Raith GmbH),* 2006.

[8] A. Tilke, M. Vogel, F. Simmel, A. Kriele, R. H. Blick, H. Lorenz, D. A. Wharam and J. P. Kotthaus, "Low-energy electron-beam lithography using calixarene," *Journal of Vacuum Science & Technology B: Microelectronics and Nanometer Structures,* vol. 17, pp. 1594-1597, 1999.

[9] H. Yang, L. Fan, A. Jin, Q. Luo, C. Gu and Z. Cui, "Low-energy electron-beam lithography of ZEP-520 positive resist," in *1st IEEE International Conference on Nano Micro Engineered and Molecular Systems, 1st IEEE-NEMS, January 18, 2006 - January 21,* 2006, pp. 391-394.

[10] T. Yoshimoto, S. H. Hwang, K. H. Kim, D. J. Seong, D. W. Kim, Y. C. Kim, S. J. Ahn and H. S. Kim, "Nano patterning fabrication by low energy microcolumn lithography," in *Optoelectronic Integrated Circuits IX, January 22, 2007 - January 24,* 2007, pp. SPIE.

[11] S. Gorelick, J. Vila-Comamala, V. A. Guzenko, R. Barrett, M. Salome and C. David, "High-efficiency Fresnel zone plates for hard X-rays by 100 keV e-beam lithography and electroplating," *Journal of Synchrotron Radiation,* vol. 18, pp. 442-6, 05, 2011.

[12] S. Gorelick, J. Vila-Comamala, V. A. Guzenko and C. David, "High aspect ratio nanostructuring by high energy electrons and electroplating," *Microelectronic Engineering,* vol. 88, pp. 2259-2262, 2011.

[13] E. D. Liu and T. Prescop, "Optimization of e-beam landing energy for EBDW," in *Alternative Lithographic Technologies III,* 2011, pp. 79701S (10 pp.).

[14] H. G. Craighead, R. E. Howard, L. D. Jackel and P. M. Mankiewich, "10-nm linewidth electron beam lithography on GaAs," *Appl. Phys. Lett.,* vol. 42, pp. 38-40, 1983.

[15] EEE Department, The University of Sheffield. EBL principles of operation. *2011(Aug. 8),* 2011). Available: http://www.shef.ac.uk/eee/research/ebl/principles.html.

[16] M. A. Mohammad, S. K. Dew, K. Westra, P. Li, M. Aktary, Y. Lauw, A. Kovalenko and M. Stepanova, "Nanoscale resist morphologies of dense gratings using electron-beam lithography," *Journal of Vacuum Science and Technology B: Microelectronics and Nanometer Structures,* vol. 25, pp. 745-753, 2007.

[17] S. Yasin, D. G. Hasko and H. Ahmed, "Fabrication of <5 nm width lines in poly(methylmethacrylate) resist using a water:isopropyl alcohol developer and ultrasonically-assisted development," *Appl. Phys. Lett.,* vol. 78, pp. 2760-2762, 2001.

[18] David J. Grant. Electron-beam lithography: From past to present. University of Waterloo. August 5, 2003)Available: http://www.davidgrant.ca/electron_beam_lithography_past_and_present.

[19] R. A. Pethrick and K. E. Rankin, "Quantitative investigation of factors influencing the efficiency of development of electron beam resists," *Microelectronic Engineering,* vol. 26, pp. 141-153, 1995.

[20] E. A. Dobisz, S. L. Brandow, E. Snow and R. Bass, "Atomic force microscope studies of nanolithographic exposure and development of

polymethylmethacrylate," *Journal of Vacuum Science & Technology B: Microelectronics Processing and Phenomena,* vol. 15, pp. 2318-2318, 1997.

[21] E. A. Dobisz, "Resist materials and nanolithography," *Mater. Res. Soc. Symp. Proc.,* vol. 584, pp. 85-96, 29 November 1999 through 2 December 1999, 2000.

[22] E. A. Dobisz, S. L. Brandow, R. Bass and J. Mitterender, "Effects of molecular properties on nanolithography in polymethyl methacrylate," *Journal of Vacuum Science and Technology B: Microelectronics and Nanometer Structures,* vol. 18, pp. 107-111, 2000.

[23] A. De Silva, L. K. Sundberg, H. Ito, R. Sooriyakumaran, R. D. Allen and C. K. Ober, "A fundamental study on dissolution behavior of high-resolution molecular glass photoresists," *Chem. Mater.,* vol. 20, pp. 7292-7300, 2008.

[24] D. L. Olynick, P. D. Ashby, M. D. Lewis, T. Jen, H. Lu, J. A. Liddle and W. Chao, "The link between nanoscale feature development in a negative resist and the hansen solubility sphere," *J. Polym. Sci. Part B,* vol. 47, pp. 2091-2105, 2009.

[25] X. Huang, G. H. Bernstein, G. Bazan and D. A. Hill, "Spatial density of lines exposed in poly(methylmethacrylate) by electron beam lithography," *Journal of Vacuum Science & Technology A: Vacuum, Surfaces, and Films,* vol. 11, pp. 1739-1744, 1993.

[26] A. Jouve, J. Simon, A. Pikon, H. Solak, C. Vannuffel and J. -. Tortai, "Overcoming pattern collapse on e-beam and EUV lithography," in *Advances in Resist Technology and Processing XXIII, Febrary 20, 2006 - Febrary 22,* 2006, pp. SPIE.

[27] A. Jouve, J. Simon, L. Gonon and J. H. Tortai, "Geometry impact on ultrahigh resolution pattern collapse," *Journal of Vacuum Science and Technology B: Microelectronics and Nanometer Structures,* vol. 25, pp. 2504-2507, 2007.

[28] J. Shin and F. Cerrina, "Line edge roughness characterization using nanotubed-AFM and SEM," in *2002 International Microprocesses and Nanotechnology Conference,* 2002, pp. 12-13.

[29] R. F. Pease and S. Y. Chou, "Lithography and other patterning techniques for future electronics," *Proc IEEE,* vol. 96, pp. 248-270, 2008.

[30] K. Matsuda, S. Ushio, Y. Hirokawa, T. Gotou and T. Kaneko, "A highly sensitive inorganic resist for directly fabricating thermally stable oxide pattern on Si substrate by low-energy electron-beam direct writing," *Japanese Journal of Applied Physics,* vol. 50, 2011.

[31] R. Capasso, L. Petti, P. Mormile, M. De Laurentis, A. Irace and G. Breglio, "Electron beam lithography for nanofabrication of metal induced bragg reflectors," in *Bioelectronics, Biomedical, and Bioinspired Systems V; and Nanotechnology V, April 18, 2011 - April 20,* 2011, pp. The Society of Photo-Optical Instrumentation Engineers (SPIE).

[32] F. Lehmann, G. Richter, T. Borzenko, V. Hock, G. Schmidt and L. W. Molenkamp, "Fabrication of sub-10-nm Au-Pd structures using 30 keV electron beam lithography and lift-off," *Microelectronic Engineering,* vol. 65, pp. 327-33, 03, 2003.

[33] F. Yaghmaie, J. Fleck, A. Gusman and R. Prohaska, "Improvement of PMMA electron-beam lithography performance in metal liftoff through a poly-imide bi-layer system," *Microelectron Eng,* vol. 87, pp. 2629-2632, 2010.

[34] M. S. M. Saifullah, H. Namatsu, T. Yamaguchi, K. Yamazaki and K. Kurihara, "Spin-coatable Al2O3 resists in electron beam nanolithography," *Proc SPIE Int Soc Opt Eng,* vol. 3678, pp. 633-642, 1999.

[35] A. Spott, Y. Liu, T. Baehr-Jones, R. Ilic and M. Hochberg, "Silicon waveguides and ring resonators at 5.5 m," *Appl. Phys. Lett.,* vol. 97, pp. 213501 (3 pp.), 11/22, 2010.

[36] H. C. George, A. O. Orlov and G. L. Snider, "Substrate effects on metal-oxide single electron transistors electrometer measurements," in *2010 68th Annual Device Research Conference (DRC 2010),* 2010, pp. 109-10.

[37] M. A. Mohammad, T. Fito, J. Chen, M. Aktary, M. Stepanova and S. K. Dew, "Interdependence of optimum exposure dose regimes and the kinetics of resist dissolution for electron beam nanolithography of polymethylmethacrylate," *Journal of Vacuum Science and Technology B: Microelectronics and Nanometer Structures,* vol. 28, pp. L1-L4, 2010.

[38] M. Aktary, M. Stepanova and S. K. Dew, "Simulation of the spatial distribution and molecular weight of polymethylmethacrylate fragments in electron beam lithography exposures," *Journal of Vacuum Science and Technology B: Microelectronics and Nanometer Structures,* vol. 24, pp. 768-779, 2006.

[39] K. -. Schock, F. E. Prins, S. Strahle and D. P. Kern, "Resist processes for low-energy electron-beam lithography," *Journal of Vacuum Science & Technology B: Microelectronics Processing and Phenomena,* vol. 15, pp. 2323-2323, 1997.

[40] C. W. Lo, M. J. Rooks, W. K. Lo, M. Isaacson and H. G. Craighead, "Resists and processes for 1 kV electron beam microcolumn lithography," *Journal of Vacuum Science and Technology B: Microelectronics and Nanometer Structures,* vol. 13, pp. 812-820, 1995.

[41] L. K. Mun, D. Drouin, E. Lavallee and J. Beauvais, "The impact of charging on low-energy electron beam lithography," *Microscopy and Microanalysis,* vol. 10, pp. 804-9, 12, 2004.

[42] J. Ingino, G. Owen, C. N. Berglund, R. Browning and R. F. W. Pease, "Workpiece charging in electron beam lithography," *Journal of Vacuum Science & Technology B (Microelectronics and Nanometer Structures),* vol. 12, pp. 1367-71, 05, 1994.

[43] M. Bai, R. F. W. Pease, C. Tanasa, M. A. McCord, D. S. Pickard and D. Meisburger, "Charging and discharging of electron beam resist films," *Journal of Vacuum Science and Technology B: Microelectronics and Nanometer Structures,* vol. 17, pp. 2893-2896, 1999.

[44] M. A. Mohammad, T. Fito, J. Chen, S. Buswell, M. Aktary, M. Stepanova and S. K. Dew, "Systematic study of the interdependence of exposure and development conditions and kinetic modelling for optimizing low-energy electron

beam nanolithography," *Microelectronic Engineering,* vol. 87, pp. 1104-1107, 2010.

[45] W. Bruenger, E. -. Kley, B. Schnabel, I. Stolberg, M. Zierbock and R. Plontke, "Low energy lithography; energy control and variable energy exposure," *Microelectronic Engineering,* vol. 27, pp. 135-138, 1995.

[46] C. Han, H. Kim, J. Kim and K. Chun, "Low energy electron beam lithography with microcolumn," in *2004 International Microprocesses and Nanotechnology Conference, October 26, 2004 - October 29,* 2004, pp. 112-113.

[47] P. Kruit and A. M. Gheidari, "Multi-electron beam systems," in *2009 22nd International Vacuum Nanoelectronics Conference (IVNC2009),* 2009, pp. 89-90.

[48] A. Ueda, Y. Nishibayashi and T. Imai, "Development and evaluation of a diamond electron source for electron beam instruments," *Diamond and Related Materials,* vol. 18, pp. 854-859, 2009.

[49] L. P. Muray, C. S. Silver and J. P. Spallas, "Sub- 100-nm lithography with miniature electron beam columns," *Journal of Vacuum Science and Technology B: Microelectronics and Nanometer Structures,* vol. 24, pp. 2945-2950, 2006.

[50] R. Galler, K. -. Choi, M. Gutsch, C. Hohle, M. Krueger, L. E. Ramos, M. Suelzle and U. Weidenmueller, "Geometrically induced dose correction: Method and performance results," in *27th European Mask and Lithography Conference,* Dresden, 2011, .

[51] M. A. Mohammad, C. Guthy, S. Evoy, S. K. Dew and M. Stepanova, "Nanomachining and clamping point optimization of silicon carbon nitride resonators using low voltage electron beam lithography and cold development,"

Journal of Vacuum Science and Technology B: Microelectronics and Nanometer Structures, vol. 28, pp. C6P36-C6P41, 2010.

[52] Mohammad Ali Mohammad, Mustafa Muhammad, Steven K. Dew, Maria Stepanova, "Fundamentals of electron beam exposure and development," in *Nanofabrication: Techniques and Principles*, 1st ed., Maria Stepanova and Steven Dew, Ed. Springer, 2011, pp. 11-41.

[53] M. Yan, S. Choi, K. R. V. Subramanian and I. Adesida, "The effects of molecular weight on the exposure characteristics of poly(methylmethacrylate) developed at low temperatures," *J Vac Sci Technol B Microelectron Nanometer Struct,* vol. 26, pp. 2306-2310, 2008.

[54] B. Cord, J. Lutkenhaus and K. K. Berggren, "Optimal temperature for development of poly(methylmethacrylate)," *Journal of Vacuum Science and Technology B: Microelectronics and Nanometer Structures,* vol. 25, pp. 2013-2016, 2007.

[55] L. E. Ocola and A. Stein, "Effect of cold development on improvement in electron-beam nanopatterning resolution and line roughness," *Journal of Vacuum Science and Technology B: Microelectronics and Nanometer Structures,* vol. 24, pp. 3061-3065, 2006.

[56] T. Yamaguchi and H. Namatsu, "Effect of developer molecular size on roughness of dissolution front in electron-beam resist," *Journal of Vacuum Science and Technology B: Microelectronics and Nanometer Structures,* vol. 22, pp. 1037-1043, 2004.

[57] S. Yasin, D. G. Hasko, M. N. Khalid, D. J. Weaver and H. Ahmed, "Influence of polymer phase separation on roughness of resist features," *Journal of Vacuum Science and Technology B: Microelectronics and Nanometer Structures,* vol. 22, pp. 574-578, 2004.

[58] Q. Hang, D. A. Hill and G. H. Bernstein, "Efficient removers for poly(methylmethacrylate)," *Journal of Vacuum Science and Technology B: Microelectronics and Nanometer Structures,* vol. 21, pp. 91-97, 2003.

[59] B. Miller-Chou and J. L. Koenig, "A review of polymer dissolution," *Progress in Polymer Science (Oxford),* vol. 28, pp. 1223-1270, 2003.

[60] S. Yasin, D. G. Hasko and H. Ahmed, "Comparison of MIBK/IPA and water/IPA as PMMA developers for electron beam nanolithography," in *Micro and Nano Engineering 2001, September 16, 2001 - September 19,* 2002, pp. 745-753.

[61] D. G. Hasko, S. Yasin and A. Mumtaz, "Influence of developer and development conditions on the behavior of high molecular weight electron beam resists," *Journal of Vacuum Science and Technology B: Microelectronics and Nanometer Structures,* vol. 18, pp. 3441-3444, 2000.

[62] L. Masaro and X. X. Zhu, "Physical models of diffusion for polymer solutions, gels and solids," *Progress in Polymer Science (Oxford),* vol. 24, pp. 731-775, 1999.

[63] G. Owen, "Electron lithography for the fabrication of microelectronic devices," *Reports on Progress in Physics,* vol. 48, pp. 795-851, 06, 1985.

[64] O. Dial, C. C. Cheng and A. Scherer, "Fabrication of high-density nanostructures by electron beam lithography," in *42nd International Conference on Electron, Ion, and Photon Beam Technology and Nanofabrication,* 1998, pp. 3887-90.

[65] L. E. Ocola, D. Tennant, G. Timp and A. Novembre, "Lithography for sub-60 nm resist nanostructures," *Journal of Vacuum Science and Technology B: Microelectronics and Nanometer Structures,* vol. 17, pp. 3164-3167, 1999.

[66] D. L. Goldfarb, J. J. De Pablo, P. F. Nealey, J. P. Simons, W. M. Moreau and M. Angelopoulos, "Aqueous-based photoresist drying using supercritical carbon dioxide to prevent pattern collapse," *J Vac Sci Technol B Microelectron Nanometer Struct,* vol. 18, pp. 3313-3317, 30 May 2000 through 2 June 2000, 2000.

[67] H. Namatsu, "Supercritical resist drying for isolated nanoline formation," *Journal of Vacuum Science and Technology B: Microelectronics and Nanometer Structures,* vol. 19, pp. 2709-2712, 2001.

[68] M. Haffner, A. Haug, A. Heeren, M. Fleischer, H. Peisert, T. Chasse and D. P. Kern, "Influence of temperature on HSQ electron-beam lithography," *Journal of Vacuum Science and Technology B: Microelectronics and Nanometer Structures,* vol. 25, pp. 2045-2048, 2007.

[69] I. Baek, J. Yang, W. Cho, C. Ahn, K. Im and S. Lee, "Electron beam lithography patterning of sub- 10 nm line using hydrogen silsesquioxane for nanoscale device applications," *Journal of Vacuum Science and Technology B: Microelectronics and Nanometer Structures,* vol. 23, pp. 3120-3123, 2005.

[70] M. Ishida, J. Fujita, T. Ogura, Y. Ochiai, E. Ohshima and J. Momoda, "Sub-10-nm-scale lithography using p-chloroinethyl-methoxy-calix[4]arene resist," in *Microprocesses and Nanotechnology,* 2003, pp. 3913-3916.

[71] D. Borah, M. T. Shaw, S. Rasappa, R. A. Farrell, C. O'Mahony, C. M. Faulkner, M. Bosea, P. Gleeson, J. D. Holmes and M. A. Morris, "Plasma etch technologies for the development of ultra-small feature size transistor devices," *J. Phys. D,* vol. 44, 2011.

[72] J. Manyam, M. Manickam, J. A. Preece, R. E. Palmer and A. P. G. Robinson, "Plasma etching of high-resolution features in a fullerene molecular resist," in *Advances in Resist Materials and Processing Technology XXVIII,* San Jose, CA, 2011, .

[73] M. K. Othman, H. A. Hashim, A. Yusof and A. Dolah, "Wet chemical etching of GaAs via hole using phosphoric acid mixture," *AIP Conference Proceedings,* vol. 909, pp. 161-5, 05/09, 2007.

[74] X. Han, G. Larrieu and E. Dubois, "Realization of vertical silicon nanowire networks with an ultra high density using a top-down approach," in 2010, pp. 7423-7427.

[75] A. J. Speth, A. D. Wilson, A. Kern and T. H. P. Chang, "ELECTRON-BEAM LITHOGRAPHY USING VECTOR-SCAN TECHNIQUES," *Journal of Vacuum Science and Technology,* vol. 12, pp. 1235-1239, 1975.

[76] G. Rius Suñé. Electron beam lithography for nanofabrication. 2008). Available: http://www.tdx.cat/TDX-1120108-160434.

[77] B. Wu and A. R. Neureuther, "Energy deposition and transfer in electron-beam lithography," *J Vac Sci Technol B Microelectron Nanometer Struct,* vol. 19, pp. 2508-2511, 2001.

[78] A. C. F. Hoole, M. E. Welland and A. N. Broers, "Negative PMMA as a high-resolution resist - The limits and possibilities," *Semicond Sci Technol,* vol. 12, pp. 1166-1170, 1997.

[79] I. Haller, M. Hatzakis and R. Srinivasan, "High-resolution positive resists for electron-beam exposure," *IBM Journal of Research and Development,* vol. 12, pp. 251-256, 1968.

[80] J. O. Choi, J. A. Moore, J. C. Corelli, J. P. Silverman and H. Bakhru, "Degradation of poly(methylmethacrylate) by deep ultraviolet, x-ray, electron beam, and proton beam irradiations," *Journal of Vacuum Science & Technology B: Microelectronics and Nanometer Structures,* vol. 6, pp. 2286-2289, 1988.

[81] J. A. Moore and J. O. Choi. "Degradation of poly(methyl methacrylate)," in *Radiation Effects on Polymers*Anonymous 1991, Available: http://dx.doi.org/10.1021/bk-1991-0475.ch011.

[82] Schmalz, Olaf AU, Hess, Michael AU, Kosfeld, Robert. Structural changes in poly(methyl methacrylate) during deep-etch X-ray synchrotron radiation lithography. *Angew. Makromol. Chem. 239(1),* pp. 63-79. 1996. Available: http://dx.doi.org/10.1002/apmc.1996.052390107.

[83] V. M. Bermudez, "Low-energy electron-beam effects on poly(methyl methacrylate) resist films," *Journal of Vacuum Science & Technology B (Microelectronics and Nanometer Structures),* vol. 17, pp. 2512-18, 11, 1999.

[84] Kirill Koshelev, Mohammad Ali Mohammad, Taras Fito, Ken Westra, Steven Dew and Maria Stepanova. Comparison between ZEP and PMMA resists for nanoscale electron beam lithography experimentally and by numerical modeling. *Journal of Vacuum Science & Technology B (Microelectronics and Nanometer Structures)* 2011).

[85] Andrea Gusman, Srivigyan Chandu, Frank Yaghmaie. ZEP520A – new resist for electron beam lithography. *2011(Aug. 10),* 2011). Available: http://ncnc.engineering.ucdavis.edu/pages/equipment/ZEP520A-Process.pdf.

[86] S. Long, Z. Li, X. Zhao, B. Chen and M. Liu, "Process study of ZEP520 positive electron-beam resist and its application in single-electron transistor," in *Advanced Microlithography Technologies, November 8, 2004 - November 10,* 2005, pp. 255-266.

[87] K. Yamaguchi, H. Ozaki, A. Hirao, N. Hirose, Y. Harada, Y. Uzawa, M. Sekine, S. Yoshimor and M. Kawamura, "New positive EB resist with strong resistance to plasma damage," *J. Electrochem. Soc.,* vol. 139, pp. 33-34, 1992.

[88] T. Okada, J. Fujimori, M. Aida, M. Fujimura, T. Yoshizawa, M. Katsumura and T. Iida, "Enhanced resolution and groove-width simulation in cold development of ZEP520A," *Journal of Vacuum Science and Technology B: Microelectronics and Nanometer Structures,* vol. 29, 2011.

[89] D. A. Czaplewski and L. E. Ocola, "Increased pattern transfer fidelity of ZEP 520A during reactive ion etching through chemical modifications by additional dosing of the electron beam resist," *Journal of Vacuum Science & Technology B*

(Microelectronics and Nanometer Structures), vol. 29, pp. 021601 (7 pp.), 03, 2011.

[90] H. Namatsu, Y. Takahashi, K. Yamazaki, T. Yamaguchi, M. Nagase and K. Kurihara, "Three-dimensional siloxane resist for the formation of nanopatterns with minimum linewidth fluctuations," *Journal of Vacuum Science & Technology B: Microelectronics Processing and Phenomena,* vol. 16, pp. 69-69, 1998.

[91] R. Bonam, P. Verhagen, A. Munder and J. Hartley, "Performance characterization of negative resists for sub-10-nm electron beam lithography," *J Vac Sci Technol B Microelectron Nanometer Struct,* vol. 28, pp. C6C34-C6C40, 2010.

[92] H. Namatsu, T. Yamaguchi, M. Nagase, K. Yamazaki and K. Kurihara, "Nano-patterning of a hydrogen silsesquioxane resist with reduced linewidth fluctuations," *Microelectronic Engineering,* vol. 41-42, pp. 331-334, 1998.

[93] M. Yan, J. Lee, B. Ofuonye, S. Choi, J. H. Jang and I. Adesida, "Effects of salty-developer temperature on electron-beam-exposed hydrogen silsesquioxane resist for ultradense pattern transfer," *J Vac Sci Technol B Microelectron Nanometer Struct,* vol. 28, pp. C6S23-C6S27, 2010.

[94] G. Singh, P. Stenberg, P. Vahima, M. Kuittinen, R. P. Yadav and V. Janyani, "Hydrogen silsesquioxane (HSQ): A perfect negative tone resist for developing nanostructure patterns on a silicon platform," in *Advanced Fabrication Technologies for Micro/Nano Optics and Photonics IV, January 25, 2011 - January 26,* 2011, pp. The Society of Photo-Optical Instrumentation Engineers (SPIE).

[95] M. Zhao, B. Chen, C. Xie, M. Liu and J. Nie, "Study of process of HSQ in electron beam lithography," in *5th IEEE International Conference on Nano/Micro Engineered and Molecular Systems, NEMS 2010,* Xiamen, 2010, pp. 1021-1024.

[96] D. Gil, R. Menon and H. I. Smith, "Fabrication of high-numerical-aperture phase zone plates with a single lithography exposure and no etching," in 2003, pp. 2956-2960.

[97] D. P. Mancini, K. A. Gehoski, E. Ainley, K. J. Nordquist, D. J. Resnick, T. C. Bailey, S. V. Sreenivasan, J. G. Ekerdt and C. G. Willson, "Hydrogen silsesquioxane for direct electron-beam patterning of step and flash imprint lithography templates," *Journal of Vacuum Science and Technology B: Microelectronics and Nanometer Structures,* vol. 20, pp. 2896-2901, 2002.

[98] P. Nesladek, "Challenges of the mask manufacturing approaching physical limits," *J Phys Chem Solids,* vol. 68, pp. 926-930, 2007.

[99] C. L. Frye and W. T. Collins, "Oligomeric silsesquioxanes, (HSiO3/2)n," *J. Am. Chem. Soc.,* vol. 92, pp. 5586-5588, 09/01, 1970.

[100] H. Duan, D. Winston, J. K. W. Yang, B. M. Cord, V. R. Manfrinato and K. K. Berggren, "Sub-10-nm half-pitch electron-beam lithography by using poly(methyl methacrylate) as a negative resist," in 2010, pp. C6C58-C6C62.

[101] I. Zailer, J. E. F. Frost, V. Chabasseur-Molyneux, C. J. B. Ford and M. Pepper, "Crosslinked PMMA as a high-resolution negative resist for electron beam lithography and applications for physics of low-dimensional structures," *Semiconductor Science and Technology,* vol. 11, pp. 1235-1238, 1996.

[102] W. H. Teh, C. Liang, M. Graham and C. G. Smith, "Cross-linked PMMA as a low-dimensional dielectric sacrificial layer," *J Microelectromech Syst,* vol. 12, pp. 641-648, 2003.

[103] R. Ruiz, H. Kang, F. A. Detcheverry, E. Dobisz, D. S. Kercher, T. R. Albrecht, J. J. de Pablo and P. F. Nealey, "Density Multiplication and Improved Lithography by Directed Block Copolymer Assembly," *Science,* vol. 321, pp. 936-939, August 15, 2008.

[104] G. Liu, C. S. Thomas, G. S. W. Craig and P. F. Nealey, "Integration of density multiplication in the formation of device-oriented structures by directed assembly of block copolymer-homopolymer blends," *Advanced Functional Materials,* vol. 20, pp. 1251-1257, 2010.

[105] S. Ji, C. Liu, G. Liu and P. F. Nealey, "Molecular transfer printing block copolymers," in 2010, pp. 599-609.

[106] A. Carlson and T. K. Liu, "Negative and iterated spacer lithography processes for low variability and ultra-dense integration," in *Optical Microlithography XXI, Febrary 26, 2008 - Febrary 29,* 2008, pp. The International Society for Optical Engineering (SPIE).

[107] J. K. W. Yang, Y. S. Jung, J. -. Chang, R. A. Mickiewicz, A. Alexander-Katz, C. A. Ross and K. K. Berggren, "Complex self-assembled patterns using sparse commensurate templates with locally varying motifs," *Nat. Nanotechnol.,* vol. 5, pp. 256-260, 2010.

[108] D. F. Stamatialis, M. Sanopoulou and I. Raptis, "Swelling and dissolution behavior of poly(methyl methacrylate) films in methyl ethyl ketone/methyl

alcohol mixtures studied by optical techniques," *J Appl Polym Sci,* vol. 83, pp. 2823-2834, 2002.

[109] M. J. Rooks, E. Kratschmer, R. Viswanathan, J. Katine, R. E. Fontana Jr. and S. A. MacDonald, "Low stress development of poly(methylmethacrylate) for high aspect ratio structures," *Journal of Vacuum Science and Technology B: Microelectronics and Nanometer Structures,* vol. 20, pp. 2937-2941, 2002.

[110] A. Olzierski and I. Raptis, "Development and molecular-weight issues on the lithographic performance of poly (methyl methacrylate)," in *Micro and Nano Engineering 2003, September 22, 2003 - September 25,* 2004, pp. 244-251.

[111] M. A. Mohsin and J. M. G. Cowie, "Enhanced sensitivity in the electron beam resist poly(methyl methacrylate) using improved solvent developer," *Polymer,* vol. 29, pp. 2130-2135, 1988.

[112] W. Hu, K. Sarveswaran, M. Lieberman and G. H. Bernstein, "Sub-10 nm electron beam lithography using cold development of poly(methylmethacrylate)," *Journal of Vacuum Science and Technology B: Microelectronics and Nanometer Structures,* vol. 22, pp. 1711-1716, 2004.

[113] T. Wahlbrink, D. Kupper, J. Bolten, M. Moller, M. C. Lemme and H. Kurz, "Supercritical drying for high aspect-ratio HSQ nano-structures," *Microelectronic Engineering,* vol. 84, pp. 1045-1048, 2007.

[114] H. Namatsu, K. Yamazaki and K. Kurihara, "Supercritical drying for nanostructure fabrication without pattern collapse," *Microelectronic Engineering,* vol. 46, pp. 129-132, 1999.

[115] H. Namatsu, K. Yamazaki and K. Kurihara, "Supercritical resist dryer," *Journal of Vacuum Science and Technology B: Microelectronics and Nanometer Structures,* vol. 18, pp. 780-784, 2000.

[116] T. Wahlbrink, D. Kupper, Y. M. Georgiev, J. Bolten, M. Moller, D. Kupper, M. C. Lemme and H. Kurz, "Supercritical drying process for high aspect-ratio HSQ nano-structures," *Microelectronic Engineering,* vol. 83, pp. 1124-1127, 2006.

[117] D. Kupper, D. Kupper, T. Wahlbrink, W. Henschel, J. Bolten, M. C. Lemme, Y. M. Georgiev and H. Kurz, "Impact of supercritical CO2 drying on roughness of hydrogen silsesquioxane e-beam resist," *Journal of Vacuum Science & Technology B (Microelectronics and Nanometer Structures),* vol. 24, pp. 570-4, 03, 2006.

[118] W. Chen and H. Ahmed, "Fabrication of 5-7 nm wide etched lines in silicon using 100 keV electron-beam lithography and polymethylmethacrylate resist," *Appl. Phys. Lett.,* vol. 62, pp. 1499-1501, 1993.

[119] S. Yasin, D. G. Hasko and H. Ahmed, "Fabrication of <5 nm width lines in poly(methylmethacrylate) resist using a water:isopropyl alcohol developer and ultrasonically-assisted development," *Appl. Phys. Lett.,* vol. 78, pp. 2760-2762, 2001.

[120] C. A. Mack, "*Field Guide to Optical Lithography*," *SPIE Press,* 2006.

[121] Koshelev, K. Ali Mohammad, M. Fito, T. Westra, K. L. Dew, S. K. Stepanova, M.

Comparison between ZEP and PMMA resists for nanoscale electron beam

lithography experimentally and by numerical modeling. *J. Vac. Sci. Technol. B 29(6),* pp. 06F306. 2011. Available: http://dx.doi.org/10.1116/1.3640794.

[122] W. H. Teh, C. Liang, M. Graham and C. G. Smith, "Cross-linked PMMA as a low-dimensional dielectric sacrificial layer," *J Microelectromech Syst,* vol. 12, pp. 641-648, 2003.

[123] Cord, Bryan M. (Bryan Michael). Achieving sub-10-nm resolution using scanning electron beam lithography. 2009). Available: http://hdl.handle.net/1721.1/53267.

[124] H. Koop, M. Zech, K. Karrai, D. Schnurbusch, M. Muller, T. Grundl, M. -. Amann and A. W. Holleitner, "In situ direct visualization of irradiated electron-beam patterns on unprocessed resists using atomic force microscopy," in 2010, pp. 802-805.

[125] M. Kotera and Y. Akiba, "Analysis of resist surface deformation during electron beam irradiation," *Japanese Journal of Applied Physics,* vol. 49, pp. 06GE081-06GE085, 2010.

[126] M. J. BOWDEN, "A perspective on resist materials for fine-line lithography," in *Materials for Microlithography*Anonymous American Chemical Society, 1985, pp. 39-117.

[127] W. Moreau, *Semiconductor Lithography: Principles, Practices, and Materials (Microdevices).* Plenum Press, 1989.

[128] N. Arjmandi, L. Lagae and G. Borghs, "Enhanced resolution of poly(methyl methacrylate) electron resist by thermal processing," *Journal of Vacuum Science*

and Technology B: Microelectronics and Nanometer Structures, vol. 27, pp. 1915-1918, 2009.

[129] S. Noach, M. Manevich, N. P. Eisenberg, E. P. Fokin and T. V. Mihalina, "Optical near-field and thermal nanolithography using organic dry developing photoresist," *Nanotechnology,* vol. 16, pp. 775-778, 2005.

[130] S. N. Ali, S. Ghafouri, Z. Yin, P. Froimowicz, S. Begum and M. A. Winnik, "A comparative thermogravimetric study of polymers designed as dry-developing photoresists," *European Polymer Journal,* vol. 44, pp. 4129-4138, 2008.

[131] V. Auzelyte, A. Langner and H. H. Solak, "Thermal development of a calixarene resist," *J Vac Sci Technol B Microelectron Nanometer Struct,* vol. 27, pp. 2990-2992, 2009.

[132] N. Vourdas, A. G. Boudouvis and E. Gogolides, "Plasma etch rate measurements of thin PMMA films and correlation with the glass transition temperature," *J. Phys. Conf. Ser.,* vol. 10, pp. 405-408, 2005.

[133] C. Zhang, C. Yang and D. Ding, "Deep reactive ion etching of PMMA," *Appl. Surf. Sci.,* vol. 227, pp. 139-143, 2004.

[134] H. Nabesawa, T. Hitobo, S. Wakabayashi, T. Asaji, T. Abe and M. Seki, "Polymer surface morphology control by reactive ion etching for microfluidic devices," *Sens Actuators, B Chem,* vol. 132, pp. 637-643, 2008.

[135] Veeco, "NanoScope Command Reference Manual," .

[136] H. Duan, J. Zhao, Y. Zhang, E. Xie and L. Han, "Preparing patterned carbonaceous nanostructures directly by overexposure of PMMA using electron-beam lithography," *Nanotechnology,* vol. 20, 2009.

[137] A. A. Tseng, "Recent developments in nanofabrication using ion projection lithography," *Small,* vol. 1, pp. 594-608, 2005.

[138] E. van der Drift and D.L. Maas, "Helium ion lithography," in *Nanofabrication: Techniques and Principles*, 1st ed., Maria Stepanova and Steven Dew, Ed. Springer, 2011, pp. 93-116.

[139] F. Schrempel and W. Witthuhn, "Deep light ion lithography in PMMA - A parameter study," *Nuclear Instruments & Methods in Physics Research, Section B (Beam Interactions with Materials and Atoms),* vol. 132, pp. 430-8, 11, 1997.